Geophys. Astrophys. Fluid Dynamics, Vol. 90, pp. 1–41
Reprints available directly from the publisher
Photocopying permitted by license only

INTERACTION OF A MONOPOLAR VORTEX WITH A TOPOGRAPHIC RIDGE

J. H. G. M. VAN GEFFEN and P. A. DAVIES

Department of Civil Engineering, University of Dundee, Dundee DD1 4HN, United Kingdom

(Received 22 December 1997; In final form 3 September 1998)

The interaction of a monopolar vortex with a cosine-shaped topographic ridge at the equator is investigated with a two-dimensional numerical model, where the (cyclonic) monopole has a self-induced northwest-ward motion due to the β-effect. The fate of the monopole depends on the width and height of the ridge, but, more importantly, on the orientation of the ridge. Whereas monopoles are always seen to cross an east-west or northeast-southwest ridge, a north-south ridge can cause such deformations in the monopole's shape that it either splits into two parts (where the associated secondary vortex may or may not also cross the ridge) or it is destroyed. The computations show that the monopole can only cross the top of the ridge once it has gathered sufficient positive potential vorticity at its (north)west side. The vortex achieves this by moving along the ascending side of the ridge, westward for the east-west ridge and northward for the north-south ridge, before crossing the summit.

Keywords: Vortex dynamics; rotation; topography

1. INTRODUCTION

Vortices are common features under many geophysical circumstances. Observations (see e.g., Richardson 1993a, b; Bower *et al.*, 1995; Kamenkovich *et al.*, 1996; Bograd *et al.*, 1997) have, for instance, shown the existence of several kinds of vortices in the Earth's oceans, such as Meddies, Gulf Stream eddies and anticyclones, Agulhas eddies, *etc.* These eddies are quite abundant; Richardson (1993b) estimates that there are roughly 1000 discrete eddies in the North Atlantic. The vortices move due to a combination of the latitudinal variation of the Coriolis force (the so-called β-effect) and the general

background oceanic flow. As such vortices move, they inevitably encounter submarine topographic features at the bottom of the ocean or the edges of coastal shelves.

Interactions with topographic features are known to influence the trajectories of the vortices and it is possible that the vortex is destroyed by the topography. For instance, Richardson (1993a, b) gives the example of a Meddy off the westcoast of Portugal that had a catastrophic end in the vicinity of Hyères Seamount after an estimated life time of 2.5 years. As a result, the Meddy's contents – Mediterranean water with its high salinity and pollution – was released into the Atlantic Ocean. Shapiro *et al.* (1995) report observations of a Meddy that was damaged by a collision with a group of seamounts but kept its coherent structure (though it lost some of its contents).

Eddies are thus thought to play an important role in transporting water properties within the oceans and it is therefore of interest to understand the basic mechanisms behind the interaction of a vortex with a bottom topography. In this regard, a two-layer model has been used by Kamenkovich *et al.* (1996) for studying Agulhas eddies that encounter a ridge, which showed that Agulhas eddies that cross the ridge can carry their contents far into the South Atlantic subtropical gyre. Smith and O'Brien (1983) used a two-layer model for an eddy on a coastal shelf. Such eddies move along the shore with a tendency to go onshore (offshore) for a cyclonic (anticyclonic) vortex (see also Grimshaw *et al.*, 1994). The latter tendency is caused by the β-effect (or its dynamical equivalent of a sloping bottom, with "north" towards decreasing fluid depth; see e.g., Van Heijst, 1994): a cyclonic (anticyclonic) monopole moves on the northern hemisphere to the northwest (southwest). It is also this effect that causes a cyclonic vortex to climb out of a conical valley and to the top of a hill (Carnevale *et al.*, 1991). Verron and Le Provost (1985) showed that in a flow over an isolated seamount (anti)cyclonic vortices may be formed, depending on the flow characteristics and the presence or absence of the β-effect. Ezer (1994) showed that eddies are formed in the region where the Gulf Stream passes over a chain of seamounts.

The present paper employs a simple one-layer two-dimensional (shallow water) model to study the basic features of vortex–topography interactions. As a first step in this investigation, a cyclonic monopole that encounters a smooth ridge located at the equator is

simulated, where the height and width of the ridge and its orientation are varied. The numerical model used for the simulations is outlined in Section 2. In Section 3 the effects of a topographic disturbance on an approaching vortex are discussed and a simple example is given to show that these effects are well represented by the model. The monopole used for the interaction-study and the mechanism for its motion (the β-effect) are introduced in Section 4. Sections 5 to 7 present the results of the simulations and some concluding remarks are formulated in Section 8.

2. THE NUMERICAL MODEL

This section presents in brief the basic equations that describe the evolution of a two-dimensional vorticity distribution in the presence of a bottom topography and the numerical method used for the flow simulations.

2.1. Governing Equations

In oceanic cases, typical bottom topographic disturbances induce three-dimensional motions in the surrounding flow. Assuming, however, that the vertical motions induced by the topography are small compared with the horizontal velocities, *viz.*

$$w \ll u, v, \tag{1}$$

where $\mathbf{v} = (u, v, w)$ is the relative velocity field of the flow, bottom topography can be incorporated in a two-dimensional (2D) model. With assumption (1) in mind, conservation of mass for a flow across a topography with fluid depth $H = H(x, y)$ is given by z

$$\nabla \cdot H\mathbf{v} = \frac{\partial(Hu)}{\partial x} + \frac{\partial(Hv)}{\partial y} = 0, \tag{2}$$

or

$$\nabla \cdot \mathbf{v} = -\frac{1}{H}(\mathbf{v} \cdot \nabla)H, \tag{3}$$

for an incompressible fluid (where the fluid density ρ is constant). In the case of the fluid depth H being uniform, this equation obviously reduces to the familiar form $\nabla \cdot \boldsymbol{v} = 0$. In order for the assumption of (quasi) 2D motions (1) to remain valid, H must be of order 1: the topography cannot be too high or too deep in a 2D model.

For incompressible (quasi) 2D flows across a topography, i.e. with (1) and (3), conservation of momentum can be written as

$$\frac{\mathrm{D}}{\mathrm{D}t}\left(\frac{\omega+f}{H}\right) \equiv \frac{\partial \omega}{\partial t} + H(\boldsymbol{v}\cdot\nabla)\left(\frac{\omega+f}{H}\right) = \nu\nabla^2\omega\,, \tag{4}$$

with $\mathrm{D}/\mathrm{D}t$ the material derivative, ω the relative vorticity, defined by

$$\boldsymbol{\omega} = \nabla \times \boldsymbol{v} = \omega \boldsymbol{k} = (0,0,\omega)\,, \tag{5}$$

ν the kinematic viscosity, and f the so-called Coriolis parameter

$$f = 2\Omega \sin\phi, \tag{6}$$

which describes the latitudinal (ϕ) variation of the vertical component of the Earth's angular rotation Ω. (Both H and f are assumed to be time-independent.) The ratio between large brackets in (4) is the potential vorticity:

$$\omega_p = \frac{\omega+f}{H}, \tag{7}$$

and (4) states that for inviscid fluids ω_p is conserved.

It is convenient to introduce what can be denoted the potential stream function ψ_p (denoted the "mass transport streamfunction" by Grimshaw *et al.*, 1994), defined as

$$Hu = \frac{\partial \psi_p}{\partial y}, \quad Hv = -\frac{\partial \psi_p}{\partial x}, \tag{8}$$

or, more generally

$$H\boldsymbol{v} = \nabla \times \boldsymbol{k}\psi_p = \nabla\psi_p \times \boldsymbol{k}, \tag{9}$$

which satisfies (3). With definition (9), equation (4) becomes the 2D Navier–Stokes equation in the vorticity–streamfunction formulation

$$\frac{\partial \omega}{\partial t} + J(\omega_p, \psi_p) = \nu \nabla^2 \omega, \tag{10}$$

where the Jacobian operator J:

$$J(A, B) = \frac{\partial A}{\partial x}\frac{\partial B}{\partial y} - \frac{\partial A}{\partial y}\frac{\partial B}{\partial x}, \tag{11}$$

describes the nonlinear advection effects. If this equation is made dimensionless using a typical length scale L_0 and a typical time scale T_0, the familiar Reynolds number Re appears as

$$\mathrm{Re} = \frac{L_0^2 T_0}{\nu} = \frac{\Gamma_0}{\nu}, \tag{12}$$

where Γ_0 is a typical scale for the circulation of the vorticity distribution. In what follows, all typical scales are set equal to unity, so that the Reynolds number, in effect, is $\mathrm{Re} = 1/\nu$, and all quantities are given in dimensionless units. This implies that a vortex with a translation velocity of 2, say, travels 2 length units in 1 time unit. The default fluid depth, away from any topography, is $H = 1$.

From (3), (5) and (9) follows the relation between vorticity and streamfunction

$$H\omega = -\nabla^2 \psi_p + \frac{1}{H}(\nabla H \cdot \nabla \psi_p), \tag{13}$$

which may be denoted the modified Poisson equation, to distinguish it from the regular Poisson equation

$$\omega = -\nabla^2 \psi, \tag{14}$$

valid for cases with a uniform bottom topography. Here ψ is the regular streamfunction, defined by $u = \partial\psi/\partial y$ and $v = -\partial\psi/\partial x$ and satisfying $\nabla \cdot \boldsymbol{v} = 0$.

Expanding the Coriolis parameter f around a reference latitude ϕ_0 at a sphere of radius R_s leads to (e.g., Van Heijst, 1994):

$$f = f_0 + \beta y + \mathrm{O}(y^2), \tag{15}$$

in the so-called β-plane approximation used in this paper. In (15) the local north coordinate is y and

$$f_0 = 2\Omega_s \sin\phi_0, \quad \beta = 2\Omega_s \cos\phi_0 / R_s, \tag{16,17}$$

with Ω_s the rotation rate of the sphere.

Equations (10) and (13) form the set of equations to be solved by the numerical method for given $H = H(x, y)$, f_0 and β, starting from an initial vorticity distribution $\omega(x, y, t = 0)$.

2.2. Numerical Method

The numerical method used for modelling the interactions of vortices with topography is a finite difference method that solves the two-dimensional (2D) Navier–Stokes equation in the vorticity-stream-function formulation (Van Geffen, 1998). The time integration part of the code is based on work by Orlandi and Verzicco (see e.g., Orlandi, 1990; Verzicco *et al.*, 1995). Their code has been greatly extended and improved to allow for a great variety of initial vorticity distributions, to allow for different boundary conditions, to have the possibility of following the motion of passive tracers, and to include background vorticity and/or topography if needed. That viscous effects are handled well by this method is shown by Van Geffen and Van Heijst (1998), who considered among other things the decay of a Rankine vortex.

The method applies a discretization of the equations on a rectangular grid in a rectangular domain in the x, y-plane. The time evolution in (10) is computed with an explicit third-order Runge–Kutta scheme, the viscous term $\nu\nabla^2\omega$ with a Crank–Nicolson scheme, and the nonlinear term $J(\omega_p, \psi_p)$ with the Arakawa scheme. The use of the Arakawa scheme (Arakawa, 1966) guarantees on the one hand that in the inviscid case energy, enstrophy and skew symmetry are conserved, and on the other hand that the computation has a high degree of stability.

The regular Poisson equation (14) can be solved with a relatively fast standard routine FACR (Fourier Analysis and Cyclic Reduction; see Hockney, 1965). Unfortunately, this routine cannot solve the modified Poisson equation (13) that is needed when bottom topo-

graphy is present, and a considerably slower (5–10 times) standard routine from the NAG Library has to be used (this routine is based on a multigrid method). Both routines limit the choice of the number of grid cells to 2^n ($n = 1, 2, 3, \ldots$) in either direction.

For the study of vortex–topography interactions the effect of the boundaries of the computational domain should, of course, be minimised, hence a relatively large domain is used. At the boundaries of this domain the "free-slip" condition is applied: fluid cannot move through the boundary, but it can move freely along it. Thus, the boundary is a streamline. This boundary condition has much less influence on the flow in the domain than the physically more realistic "no-slip" condition, which has zero velocities at the boundaries due to viscous friction effects. It is not possible to use periodic boundaries for this study because (i) the use of such boundaries requires that the total circulation $\int \omega dA$ in the full domain equals zero, which is not the case for the monopole used below, and (ii) the NAG routine needed for cases with topography cannot handle periodic boundaries.

3. BASIC EFFECTS OF A BOTTOM TOPOGRAPHY

The basic effects of a bottom topography can, perhaps, be explained best by assuming that the fluid is inviscid. Equation (4) then states that the potential vorticity ω_p is conserved:

$$\frac{\mathrm{D}}{\mathrm{D}t}\left(\frac{\omega + f}{H}\right) = 0. \tag{18}$$

Assume for the moment that the background rotation f is constant throughout the domain. If a vortex initially located where the fluid depth is $H = 1$, moves to the top of a ridge (fluid depth $H < 1$), then (18) states that the vortex becomes weaker. At the same time, the vortex, which has a finite horizontal size, becomes shorter (since $H < 1$) and wider (the fluid inside the vortex is incompressible). When the vortex then moves away from the ridge it becomes stronger and narrower again.

Since the numerical model employed here is two-dimensional, the squeezing and stretching of the vortex, as it climbs and descends the

topography, is of course absent. The widening and narrowing, however, and the weakening and strengthening can be seen clearly in the example discussed below, namely a Lamb dipole crossing a ridge. This example was used as one of the cases to test the numerical model in handling a bottom topography correctly. The reason that this example is a good test is that the motion of the dipole is self-induced, so that the presence of background rotation is not necessary to make it move. For such cases, the effect of the topography alone can be seen.

3.1. A Lamb Dipole Crossing a Ridge

The Lamb dipole (Lamb, 1932; see also Meleshko and Van Heijst, 1994, who showed that the Lamb dipole is a special case of the more general Chaplygin dipole) is a circular vortex structure consisting of two oppositely-signed vorticity patches with a vorticity distribution given by

$$\omega = \begin{cases} \dfrac{2U_0 k_d}{J_0(k_d R)} J_1(k_d r) \sin\theta, & r \leq R; \\ 0, & r \geq R, \end{cases} \tag{19}$$

where U_0 is the strength of the dipole, r the radial distance to the centre of the vortex, R its radius, and θ the angle with respect to the line of motion of the dipole. J_0 and J_1 are Bessel functions of the first kind and $k_d R \approx 3.8317$ is the first non-zero root of J_1. This dipole moves due to a self-induced motion along a straight line ($\theta = 0$). If the fluid is inviscid and the domain is infinite, its velocity equals U_0 and is constant in time, and the size of the vortex does not change. If there are viscous effects, the vortex gradually slows down and becomes bigger (see Van Geffen and Van Heijst, 1998). The time interval used here, however, is so short that the effects of viscosity are small.

The Lamb dipole is placed on the negative x-axis and directed towards larger x, i.e. with $U_0 > 0$. A cosine-shaped ridge is placed along the y-axis, such that the fluid depth H is given by

$$H = \begin{cases} 1 - A\cos(x\pi/w) - A, & -w < x < +w; \\ 1, & \text{elsewhere} \end{cases} \tag{20}$$

with the maximum height of the ridge (at $x = 0$) being $2A$ (A is the average height) and the width at its foot being $2w$; see Figure 1 for an illustration.

Consider, as an example, a Lamb dipole with radius $R = 0.5$ and strength $U_0 = 2$ initially at $(-1.5,0)$ and approaching the ridge given by (20) with $A = 0.2$ and $w = 1$. The domain measures 6×6 (with 128×128 grid cells) and $\mathrm{Re} = 1000$. There is no background rotation ($f = 0$), so that ω / H is constant in time, if viscosity is ignored. Hence, if H decreases, so does ω, and equally so for both dipole halves. Since the dipole reaches the ridge perpendicularly, the dipole will not move away from its initial line of motion (the x-axis).

Figure 2 shows contours of vorticity at several moments in time for the evolving dipole. It can be seen clearly from these graphs that the dipole widens and weakens as it climbs the ridge ($T = 0$ to $T = 0.75$) and becomes narrower and stronger again as it descends the ridge. When it has left the ridge ($T = 1.75$), the dipole is (almost) as small and strong as it was before reaching the ridge.

The weakening and strengthening of the dipole can also be seen in Figure 3, which shows the vorticity maximum of the dipole as a function of time. Since there is no background rotation, ω/H is constant in time as mentioned above, except for a small decrease due to viscosity. At the moment ($T = T_{\mathrm{bot}}$) when the extrema of vorticity reach the edge of the ridge, their values are ± 43.5 (initial values: ± 44.3). At the top of the ridge the fluid depth is $H = 0.6$ and it then follows from conservation of potential vorticity that the extrema of vorticity at that point are $\omega_{\mathrm{est}}\ (T_{\mathrm{top}}) = \omega_{\mathrm{est}}\ (T_{\mathrm{bot}}) * 0.6/1 = \pm 26.1$.

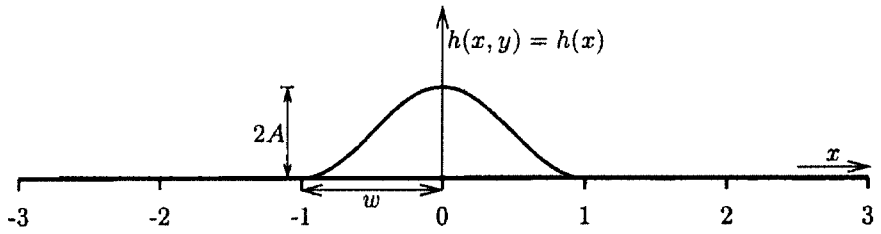

FIGURE 1 Cross-section of a cosine-shaped ridge $h(x)$ along the y-axis, given by (20); here, $w = 1$ and the maximum height of the ridge is $2A$. The fluid depth H is $H = 1 - h$. The vertical dimension is introduced here for illustrative purposes only; the numerical method is two-dimensional in the x, y-plane.

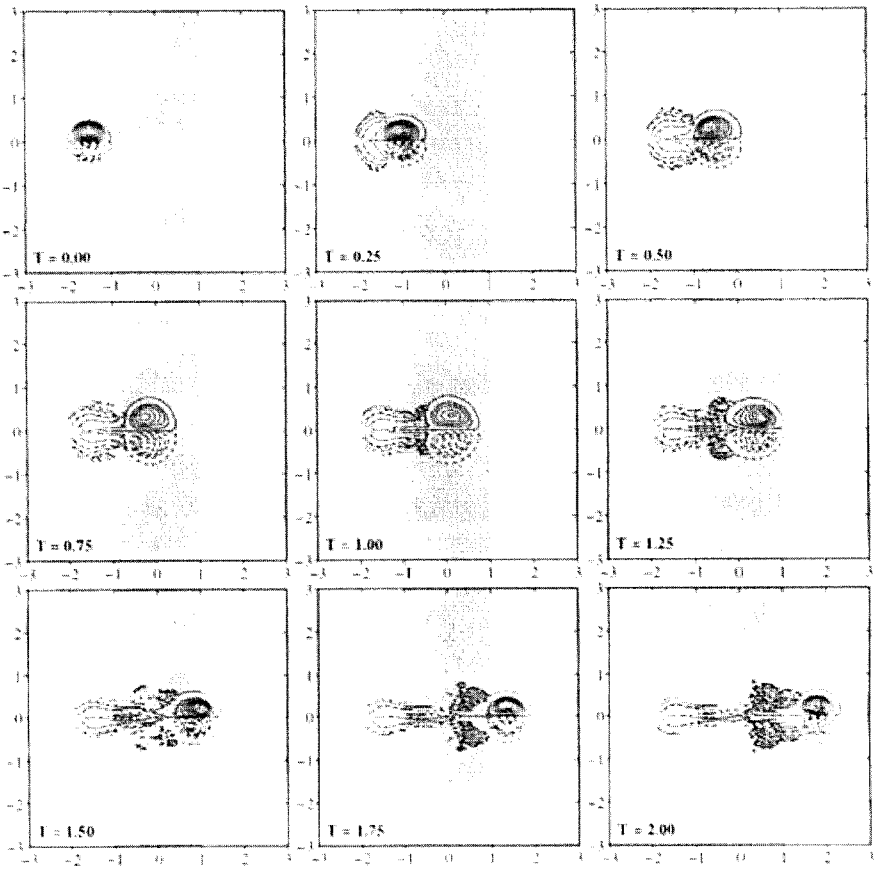

FIGURE 2 Contours of vorticity on the x, y-plane of a Lamb dipole crossing the cosine-shaped ridge (shaded region) given by (20) with $A = 0.2$ and $w = 1$. Contours are drawn at $\pm 0.1, \pm 5, \pm 10, \ldots, \pm 35, \pm 40$ (positive contours are solid, negative dashed).

This estimate is in good agreement with the results in Figure 3: the computed values are ± 25.6. Futhermore, the curve of the maximum of vorticity in Figure 3 can be fitted quite well with a cosine function, especially the part where the dipole climbs the ridge. Figure 3 also shows the Courant number CFL as a function of time, which is a measure of the maximum velocity in the domain: the dipole slows down as it becomes weaker and moves faster again as it descends the ridge. That both quantities do not return exactly to their initial value is due to the loss of some vorticity as the dipole crosses the ridge (visible as a "tail" behind the vortex in Fig. 2) and due to a small viscous decay.

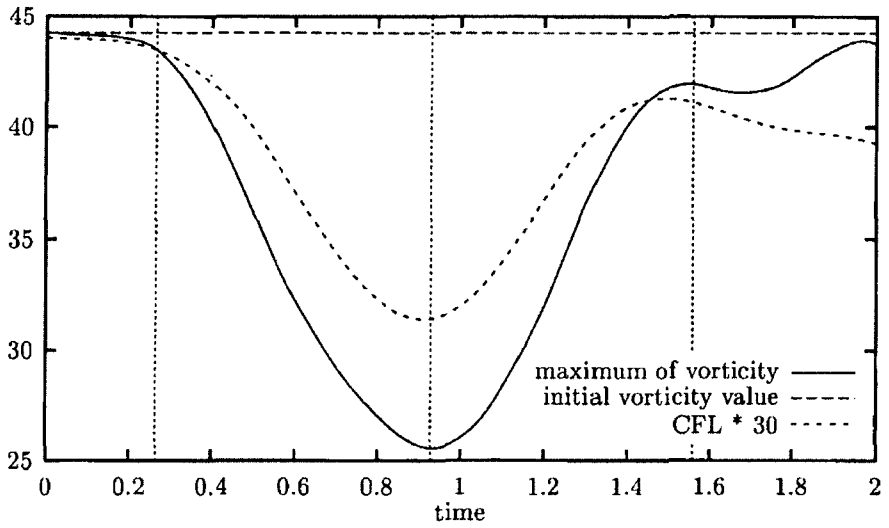

FIGURE 3 The maximum of vorticity (solid line) and the value of the Courant number CFL (dashed line) as a function of time for the dipole of Figure 2. Note that CFL has been multiplied by 30. The vertical lines represent the moments in time when the maximum of vorticity crosses the edges and the top of the ridge.

At $T = 0$ a contour of passive tracers is placed around each dipole half, at vorticity levels $\omega = \pm 0.1$. The surface of one of these contours is given in Figure 4 as a function of time, showing clearly the change in size as the dipole crosses the ridge. (Note that without topography the surface of the contour should remain constant since the fluid is incompressible.) Figure 4 also shows the divergence $\nabla \cdot \boldsymbol{v}$ of that contour, computed by integrating $\boldsymbol{v} \cdot \boldsymbol{n}$ along the contour, where $\boldsymbol{n}$ is the unit normal vector of the contour. When the dipole is away from the topography the divergence is zero, as expected from the relation given in (3). (The divergence is not exactly zero after the dipole has crossed the ridge due to the loss of some vorticity.) Both curves in Figure 4 again indicate that the dipole has (almost) returned to its original state after it has crossed the ridge.

Although the dipole is not the main subject of this paper, a few additional remarks might be in order.

For lower positive values of A the disturbance of the ridge is of course correspondingly less and for $A = 0$ there is no disturbance at all. For negative A-values, the nature of the disturbance is the same but reversed: the dipole first becomes smaller and stronger as it descends into the trough and it widens and weakens again when it

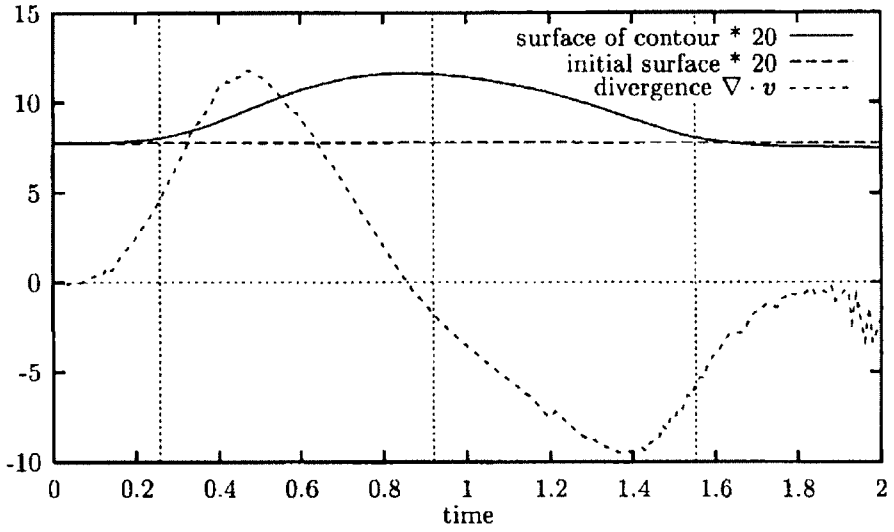

FIGURE 4 Surface (solid line) and divergence $\nabla \cdot v$ (dashed line) as a function of time for one of the contours of tracers initially at vorticity levels $\omega = \pm 0.1$ of the dipole of Figure 2. Note that the surface value has been multiplied by 20. The vertical lines are as in Figure 3.

climbs out of the trough. For values of A larger than the $A = 0.2$ used above, the disturbance is correspondingly bigger. For $A = 0.4$, for example, the dipole appears to be torn apart, though such a high ridge is unacceptable since it violates the restrictions of the model to 2D motions.

If the dipole encounters the ridge from another angle, then one half of the dipole will start climbing the ridge before the other half has reached the edge of the ridge. Consequently, the leading half will become weaker than the trailing half and the result is an asymmetric dipole that climbs the ridge along a curved path. Depending on the angle of incidence, the dipole can be rebounded by the ridge.

An asymmetric dipole is also formed when the dipole reaches the ridge perpendicularly, as above, but in the presence of a non-zero background rotation f_0. Since for this case $(\omega + f)/H$ is constant (inviscid case), the dipole halves are not affected in the same way as the dipole climbs the ridge, and one half will become weaker than the other half. Depending on the strength of the background rotation, the dipole can be deflected from its path (e.g., for $f = f_0 = 4$), or its path can be curved so much that the dipole cannot cross the ridge ($f = f_0 = 8$). For intermediate cases ($f = f_0 = 6$) the dipole can be

destroyed by the ridge, leaving a monopolar vortex from one half of the dipole, while the other half can be torn apart to form a monopole that leaves the ridge again at the ascending side (see also Carnevale *et al.*, 1988).

4. THE MONOPOLE USED FOR THE INTERACTION-STUDY

For the study of the interaction of a monopole with a topographic ridge, a Bessel monopole is used. This is a monopolar vortex of Bessel type with a vorticity distribution given by

$$\omega = \begin{cases} \dfrac{(kR)\Gamma}{2\pi R^2 J_1(kR)} J_0(kr), & r \leq R; \\ 0, & r \geq R, \end{cases} \tag{21}$$

where r is the radial distance to the centre of the vortex, R its radius, and Γ its strength or circulation, J_0 and J_1 are Bessel functions of the first kind and $kR \approx 2.4048$ is the first non-zero root of J_0. The maximum of the vorticity is located at the centre of the monopole, where J_0 equals unity. The choice for a Bessel function monopole is arbitrary, in so far that it seems best to start with a single-signed monopole with an initial vorticity distribution that is smooth and confined to a finite region. Furthermore, the vortex given by (21) is an exact, stationary solution of the inviscid vorticity equation without topography and a background rotation which is independent of location – i.e. (10) with $\nu = 0, f =$ constant and $H = 1$ – in an infinite domain, satisfying the linear relationship $\omega = k^2\psi$. The interaction processes are therefore not influenced by possible instabilities in the vortex itself.

The monopole is made to move using the β-effect and Section 4.1 outlines why a monopole moves on the β-plane and what its trajectory is. Trajectories of monopoles that encounter a ridge can then be compared with this pure β-plane trajectory. The ridge used is of the type given by (20) and sketched in Figure 1, and it is placed either along the x-axis (Section 5), the line $y = x$ (Section 6) or the y-axis (Section 7). In all cases the ridge is centred on the equator $y = 0$. The ridge has variable height and width, with the default values $A = 0.2$ and $w = 1.0$.

Unless specified otherwise, all computations presented here are made in a 20×20 domain (centred around the origin) with 256×256 grid cells; only a part of this domain is shown in plots of trajectories and contours. The background rotation is given by $f_0 = 0$ and $\beta = 0.3$. The Bessel monopole has radius $R = 0.5$ and strength $\Gamma = 4$ and is initially located at position $(3, -3)$. The time step is $\Delta t = 0.05$ and the Reynolds number is $\mathrm{Re} = 1000$. Each simulation ends at $T = 50$, unless it is at that moment unclear what the fate of the monopole is going to be, in which case the computation is continued.

Initially, a passive tracer is placed at the centre of the monopole, where the maximum of vorticity $\omega_{\max}$ is located. If the monopole moves on a pure β-plane this tracer stays nicely at $\omega_{\max}$ and the tracer can be used to plot the trajectory of the monopole. If, however, the monopole crosses the ridge, the tracer is often no longer located at the true $\omega_{\max}$ and the tracer then moves around $\omega_{\max}$. Thus, for such cases, the tracer cannot be used to track the monopole and $\omega_{\max}$ itself must be used. Since $\omega_{\max}$ (location and value) is only determined at grid points – whereas a tracer can move between grid points – a plot of $\omega_{\max}$ necessarily shows steps from grid point to grid point. This obscures the effects being studied and therefore a running average over 20 time steps is used in graphs like Figures 7 and 8.

4.1. A Bessel Monopole on a Pure β-plane

In the absence of any background vorticity (i.e. $f = 0$ and $H = 1$), a single circular monopole will remain fixed at a certain position: it possesses no self-propelling mechanism and all it does is rotate about its centre. Note that a monopole placed in a finite domain moves around the centre of the domain due to the presence of the boundaries, as discussed by Van Geffen *et al.* (1996). To minimise this effect in the computations presented in this paper, the domain is made large relative to the size of the monopole.

On a pure β-plane (with $H = 1$), however, the situation is essentially different. As the monopole rotates, fluid parcels are advected around its centre and conservation of potential vorticity then results in the creation of relative vorticity. The lowest order term in β causes a westward drift of the vortex, and the next term adds a north- or south-ward component. As a result of this, a cyclonic (anticyclonic)

monopole moves to the north-west (south-west) on the northern hemisphere. It is this effect that is used below to make a monopole cross a topography. For more about the characteristics of the motion of a monopole on a β-plane, the reader is referred to McWilliams *et al.* (1986), Carnevale *et al.* (1991), Korotaev and Fedotov (1994), Sutyrin *et al.* (1994), Van Heijst (1994), and references therein.

The motion to the north-west of a cyclonic (positive) Bessel monopole can be seen in Figure 5 – a simulation carried out in order to provide a reference with which the simulation of the interaction of a Bessel monopole with a ridge (see below) can be comparted. Figure 5 shows the trajectories of such a monopole until $T = 50$ for Re = 1000 and Re = 10,000. The two trajectories do not differ significantly, as can also be seen from the straight-line fits through the data of these simulations. The difference that is visible is due to the faster decay of the monopole at Re = 1000, as a result of which it moves slower than the monopole at Re = 10,000. Figure 5 also shows what the trajectory of such a monopole would be in the absence of any background rotation, i.e. the motion due to the presence of the boundaries cf. Van Geffen *et al.*, 1996). Clearly, the overall motion of the monopoles on

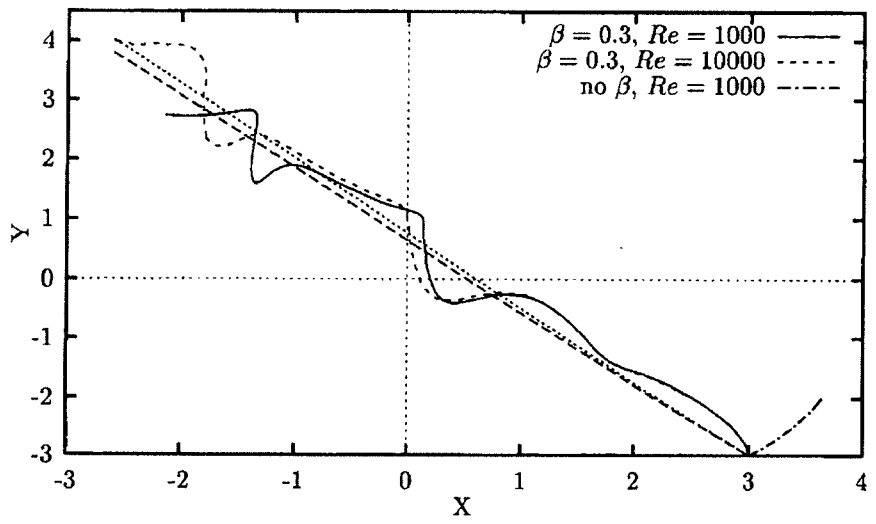

FIGURE 5 Trajectories of a Bessel monopole on a β-plane for Re = 1000 (solid line) and for Re = 10,000 (short-dashed line). The two straight lines are fits through the data points of the curves. The dot-dashed line to the right shows the trajectory of the monopole in the absence of a β-effect.

the β-plane is due to the presence of the β-effect and the effects of the boundaries are negligible.

The path the monopole follows is not a straight line. The reason for this is that as the vortex moves it sheds vorticity in the form of Rossby-waves and the vortex interacts with these Rossby-waves. Such interactions lead to somewhat more complicated trajectories. These Rossby-waves are visible in the contour plots shown in Figure 6. The larger the value of β, the faster the monopole sheds vorticity in the form of Rossby-waves, and hence the more bends the trajectory of the monopole shows. Trajectories like those shown in Figure 5 have also been observed in laboratory experiments, where the β-effect can be mimicked with a sloping bottom boundary in a rotating tank, with the north direction being oriented towards decreasing fluid depth (Carnevale *et al.*, 1991; Van Heijst, 1994). Using a sloping bottom in the numerical model with $\beta = 0$ also leads to trajectories similar those in Figure 5.

The size of the domain does not have a significant influence on the direction of the motion of the monopole on the β-plane: it moves to the northwest along a trajectory such as shown in Figure 5. The Rossby-waves shed by the moving vortex are confined to the finite-sized computational domain and "reflect" at the boundaries back into the domain. A domain of different size thus means that the interaction of the monopole with the Rossby-waves is different, which leads to a difference in the number and location of the bends in the trajectory only, not in the overall direction of motion. A linear fit through the trajectory data as in Figure 5 shows that for a 20×20, 30×30 and 40×40 the average motion is the same to within 0.5%. A 10×10 domain shows a much larger difference (5%) and initially a clear tendency of the monopole to go to the north-east due to the boundaries. Hence, a 20×20 domain is sufficiently large to neglect boundary effects.

For different values of the strength Γ of the monopole, the main difference is the distance the monopole travels in a certain time interval: the larger the value of Γ, the faster the monopole moves; the number of bends in its trajectory is not affected significantly.

The north-west motion of the monopole can be observed for a wide range of β-values and the trajectories lie around that in Figure 5. For very small β (say $\beta = 0.01$) the monopole first tends to go to the north-

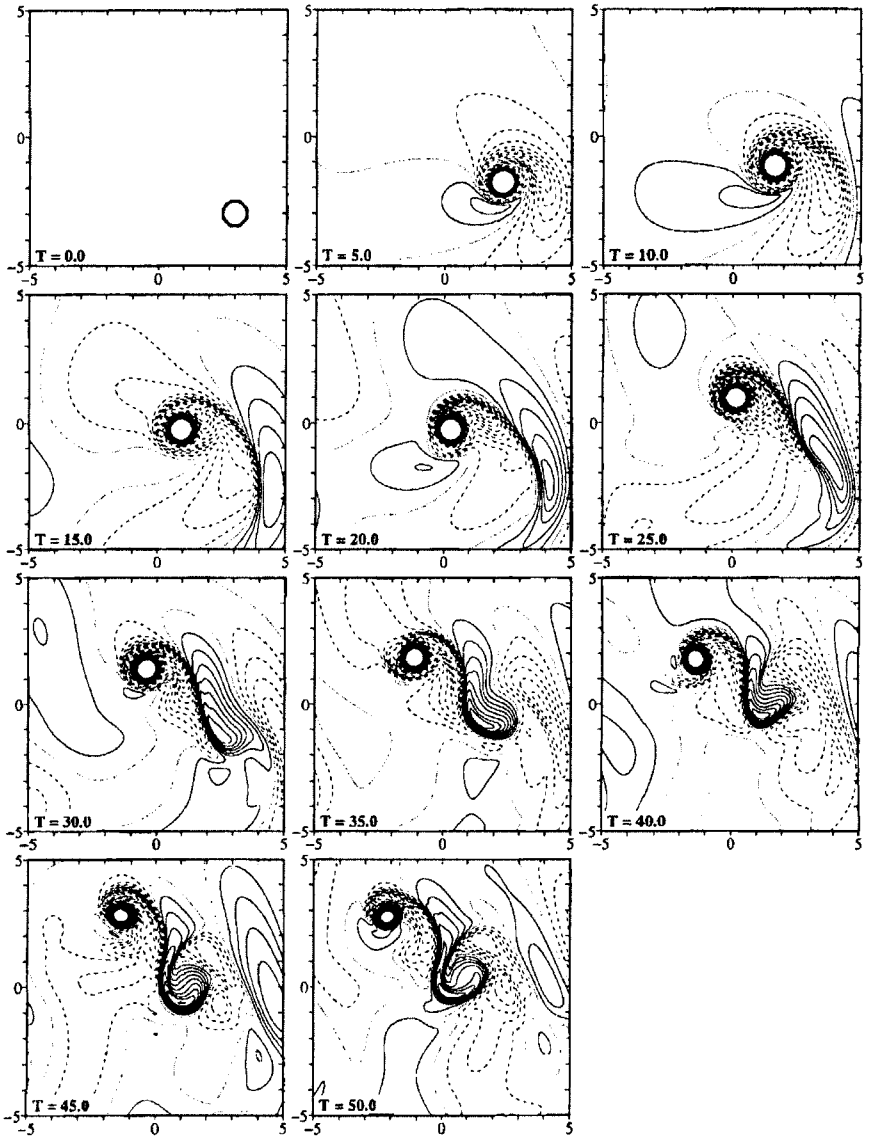

FIGURE 6 Contours of vorticity of the x, y-plane of a Bessel monopole and of the Rossby-waves it leaves behind as it moves on a β-plane for $\mathrm{Re} = 1000$; its trajectory is shown in Figure 5. Contours are drawn at intervals of 0.1 between -2.0 and 2.0; positive contours are solid, negative dashed, and the zero contour is dotted. Note that in this and following plots only the central part of the computational domain is shown.

east, a motion induced by the boundaries (cf. the dash-dotted line in Fig. 5) but it quickly turns to the north-west. For low β, the monopole moves slower than the case shown in Figure 5. For larger β-values the monopole loses vorticity (as Rossby-waves) faster, and hence it travels

slower than in Figure 5. For $\beta = 1$ the monopole decays so fast that it disappears between $T = 45$ and 50.

In the following sections, where the monopole encounters a topographic ridge, the domain size (20×20), the strength of the monopole ($\Gamma = +4$) and the β-parameter ($\beta = 0.3$) are not varied.

5. A RIDGE ALONG THE x-AXIS

Consider first of all a ridge of the type given by (20) but oriented along the x-axis, with $A = 0.2$ and $\omega = 1.0$. Figure 7 shows the trajectory of a Bessel monopole that encounters this ridge as it travels to the north-west under the action of the β-effect. The same graph shows for comparison the trajectory of the monopole in the absence of the ridge (as in Fig. 5, Re = 1000): though the trajectory is changed by the ridge, the position at $T = 50$ is seen to be almost the same for both cases. The monopole travels first more to the north than without a ridge. When it has reached the ridge, it climbs the ridge somewhat, then travels westward along the ridge, before it crosses over the top. Figure 8 shows that the monopole becomes weaker during this time interval, and then slightly stronger again as it descends the ridge

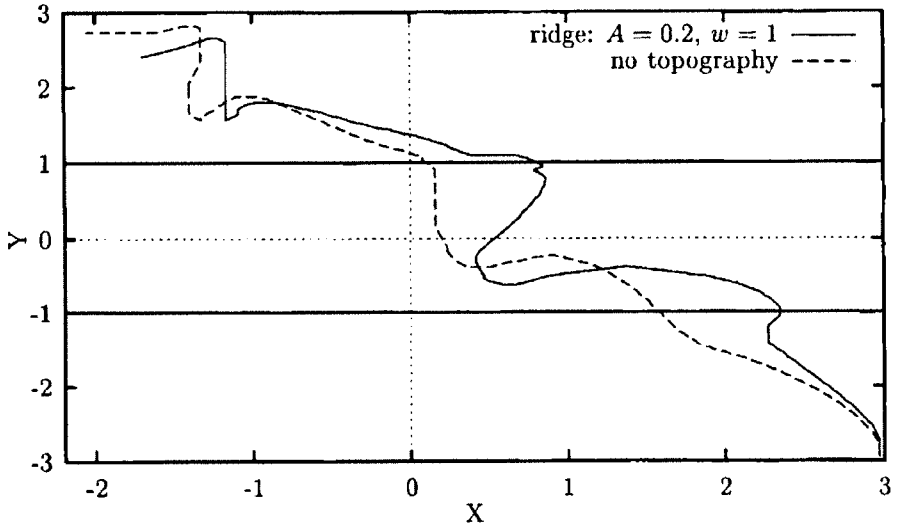

FIGURE 7 Trajectory of the maximum of vorticity of a Bessel monopole that encounters a ridge like (20) along the x-axis with $A = 0.2$ and $w = 1$ (solid line) and its trajectory in the absence of the ridge (dashed line). The thick horizontal lines mark the edges of the ridge.

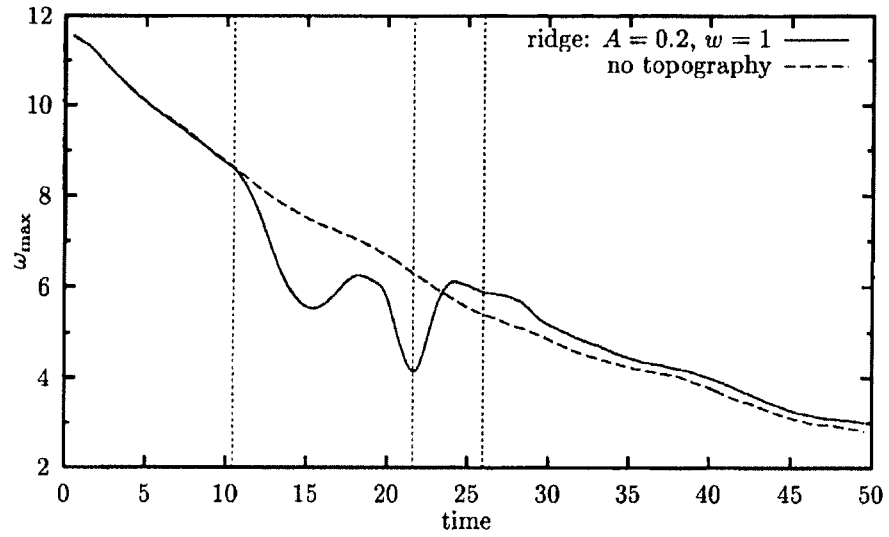

FIGURE 8 The maximum of vorticity as a function of time of the Bessel monopole whose trajectory is shown in Figure 7. The vertical lines represent the moments in time when the maximum of vorticity crosses the edges and the top of the ridge.

somewhat. The vorticity reaches a minimum value when the monopole crosses the top of the ridge. As soon as it descends along the north-side of the ridge, the monopole becomes stronger again. When it has left the ridge, it continues its normal β-induced, north-west motion. From Figure 8 it is clear that the maximum of vorticity is then even somewhat larger than expected from the viscous decay of the monopole in the absence of a topography.

Figure 9 presents the evolution of the monopole by way of contour plots of vorticity (see Fig. 6 for the same evolution without topography). The graph of $T = 15$ indicates that when the monopole travels westward along the ridge its core becomes distorted to an elliptic shape for a while. At closer inspection (not shown) the monopole appears to shed some vorticity at one tip of the ellipse. At about $T = 20$ the monopole is roughly circular again and it crosses the top of the ridge.

This process becomes clearer if the time evolution of the potential vorticity ω_p, as defined by (7), is considered. Initially, at $T = 0$, sufficiently far from the ridge and the vortex, the contours of potential vorticity are all equidistant from each other and parallel to the x-axis, since $\omega_p = \beta y$ there; the north direction is solely determined by β and is in the positive y-direction. The presence of the ridge deforms this

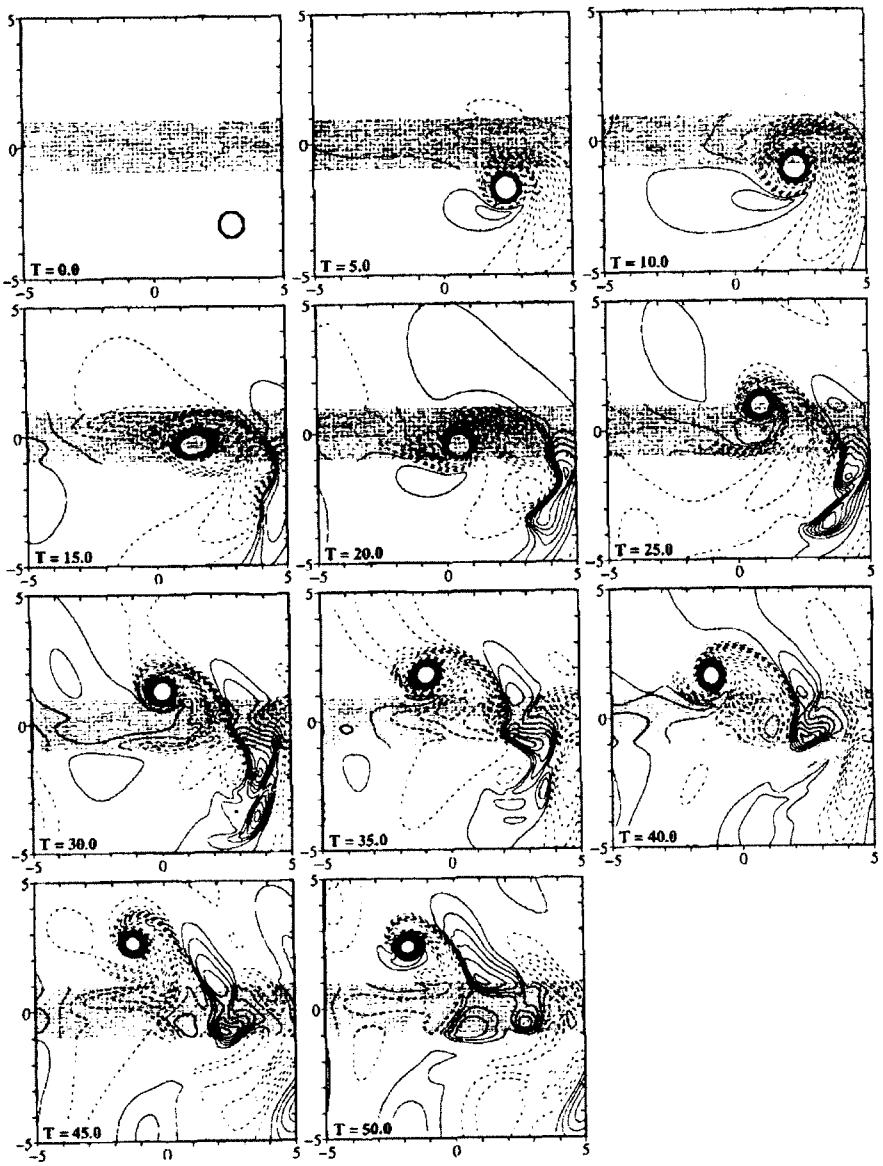

FIGURE 9 Contours of vorticity on the x,y-plane of a Bessel monopole that encounters a ridge along the x-axis (shaded region); its trajectory is shown in Figure 7. Contour levels as in Figure 6.

equidistant pattern since the topography introduces a local north in the direction of decreasing fluid depth. On the south side of the ridge the local north is therefore parallel to the β-induced north, and at the other side of the ridge the local north is anti-parallel to the β-induced north. Since the β-effect is much stronger than the effect of the ridge, the overall north direction remains the positive y-direction, but the

contours of potential vorticity are no longer equidistant from each other over the topography. It is this property that disturbs the monopole's trajectory.

Figure 10 shows contours of potential vorticity ω_p of the evolving monopole for the crucial period between $T = 12$ and $T = 23$ when the

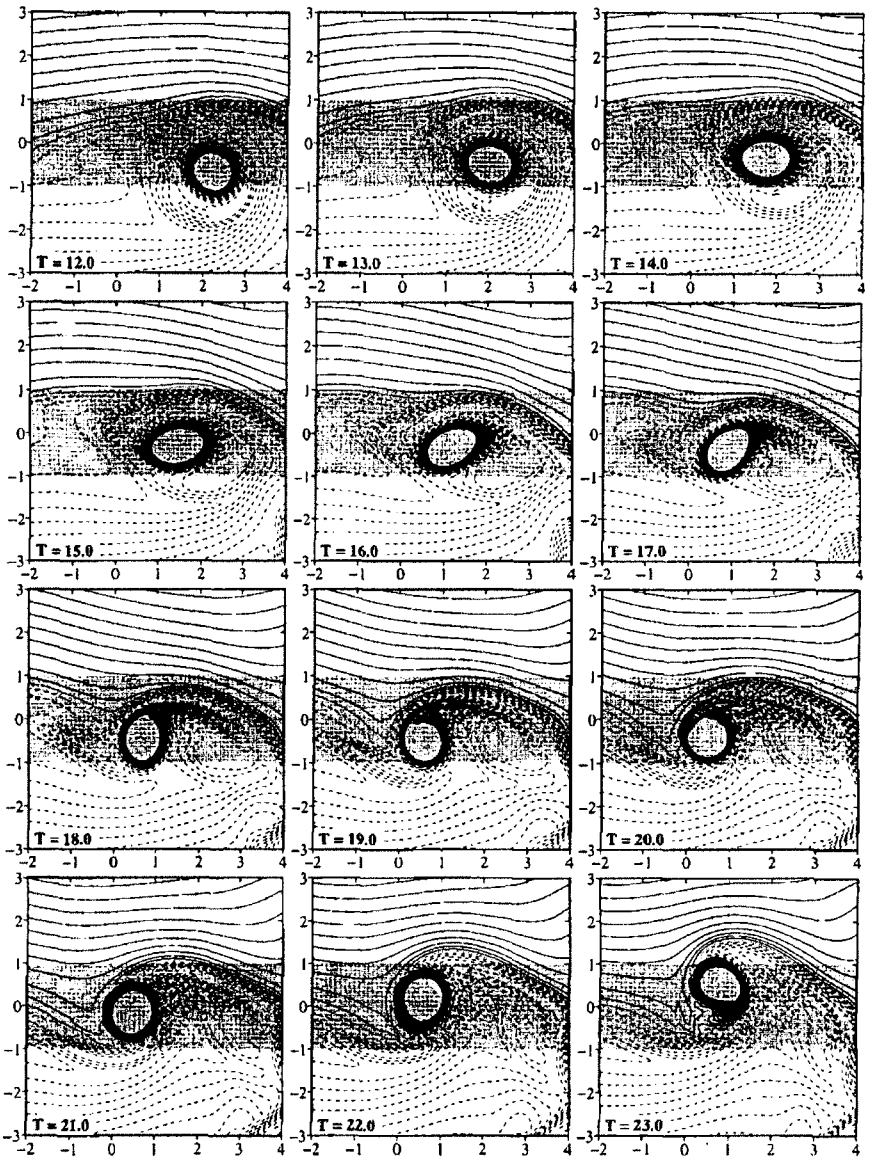

FIGURE 10 Contours of potential vorticity on the x, y-plane of the evolving monopole of Figure 9 during the period it crosses the ridge (shaded region). Contours are drawn at intervals of 0.1 between $+1.0$ and -1.0; positive contours are solid, negative dashed, and the zero contour is dotted.

ridge effect is strong. When the monopole reaches the ridge it is surrounded by negative ω_p, with a rather large gradient at its north-side. Evidently, this configuration prevents the monopole from going further north and it travels westward along the ridge. This motion occurs because of the westward drift caused by the lowest order term in β (Section 4.1) and also because of the presence of so much negative ω_p. The negative potential vorticity makes the monopole somewhat elliptic and then more circular again. Meanwhile, the monopole rolls up the ω_p-contours and pulls positive ω_p-values southward and to itself. At $T = 20$ there is positive ω_p close to the north-west side of the monopole and the latter can then cross the top of the ridge and descend at the other side of the ridge. Evidently, the negative potential vorticity temporarily forms a barrier for the (positive) monopole until the monopole is able to shed it. Once there is enough positive potential vorticity west of the monopole – i.e. left of the monopole seen with respect to the orientation of the ridge – the monopole can cross the ridge.

The degree of the influence of the ridge on the monopole depends on its characteristics A and w (and its shape, of course, but that is kept as in Fig. 1). As seems intuitively obvious, the larger the value of A, the more the trajectory differs from the trajectory it follows when there is no topography. For $A = 0.25$ the position at $T = 50$ differs nearly one length unit in the x-direction, indicating that a ridge with $A = 0.25$ might be too large for a model assuming two-dimensional motions.

If the ridge is wider than in Figure 7, the monopole crosses the ridge more to the right (east) and ends up more to the right at $T = 50$. If the ridge is narrower the opposite takes place: the monopole travels more to the west along the ridge before it crosses the top, and at $T = 50$ the monopole has a position more to the west. It thus seems that a ridge of $w \approx 1$ results in a trajectory most similar to the trajectory in the absence of the ridge. The reason for this difference in behaviour for different w-values is not yet clear, though it appears to be linked to the value of the ratio between the size of the monopole and the width of the ridge. Examination of this point is complicated by the growth in size of the vortex due to viscous decay as it moves towards and across the ridge.

6. A RIDGE ALONG THE LINE $y=x$

The ridge discussed above has an influence on the trajectory of the monopole, but this influence is not so significant that the monopole is deformed sufficiently that it does not survive crossing the ridge. This is mainly so because the potential vorticity contours of the β-effect are only slightly displaced in the y-direction by the presence of the east-west oriented ridge.

A similar ridge oriented along the line $y = x$ gives rise to a larger deformation in the contours of ω_p and these contours are no longer parallel to the x-axis over the ridge. The result is that a monopole that reaches the ridge, starting from the same initial position, is relatively more deformed. Figure 11 shows as an example comparable trajectories for several values of the height of the ridge. These trajectories are clearly more different from the ridge-less case than is the case for a ridge along the x-axis and the positions at $T = 50$ are further apart. Compare, for instance, the trajectory for $A = 0.20$ in Figure 11 (dash-dotted line) with Figure 7: in Figure 11 the monopole performs a loop over the ridge before it leaves the ridge and

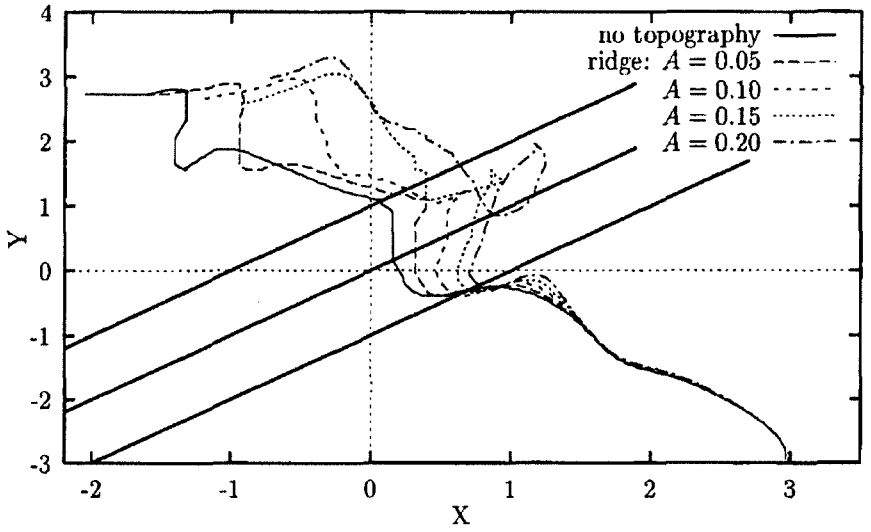

FIGURE 11 Trajectories of the maximum of vorticity of a Bessel monopole that encounters a ridge like (20) along the line $y = x$ with $w = 1$ and different values for A, as well as its trajectory in the absence of the ridge. The thick diagonal lines mark the edges and top of the ridge.

travels further north-west. A smaller loop is visible in the trajectory for $A = 0.15$ (dotted line), and a bigger one in that for $A = 0.25$ (not shown).

Again, it appears that negative potential vorticity acts as a kind of barrier for the monopole as in Figure 10: the monopole can only definitively cross the ridge when the negative ω_p patch north-west of it is no longer present and the monopole has only positive ω_p to its left, seen with respect to the ridge. With a ridge along the line $y = x$ this state is apparently more difficult to attain than with a ridge along the x-axis.

7. A RIDGE ALONG THE y-AXIS

A ridge oriented north-south appears to have a more disturbing effect on a monopole that tries to cross it: the monopole can be destroyed, in contrast to the cases discussed above. For this reason, the effect of a ridge along the y-axis is studied in more detail.

7.1. A Ridge with $A = 0.20$ and $w = 1.0$

A topographic ridge along the y-axis introduces relatively large deformation of the contours of potential vorticity from the pure β-effect, as can be seen in the top-left panel of Figure 12: the local north induced by the ridge points to decreasing fluid depth, which is perpendicular to the overall north direction from the β-effect. The result is that at the top of the ridge the ω_p-contours are squeezed towards $y = 0$, the more so the higher the ridge. Figures 12 and 13 show for a ridge given by (20) with $A = 0.2$ and $w = 1.0$ contours of potential vorticity ω_p and relative vorticity ω, respectively. As the monopole approaches the ridge, contours of potential vorticity are rolled up around it. Once the monopole is on the ascending (east) side of the ridge, at $T = 20$, it starts to move to the north along the ridge. This direction of motion is, at first sight, unexpected since the local west direction induced by the ridge is pointing to the south. It would therefore seem logical that the monopole travels to the south (as it travels to the local west in Fig. 10). But this is apparently prevented by the presence of negative ω_p south of the monopole.

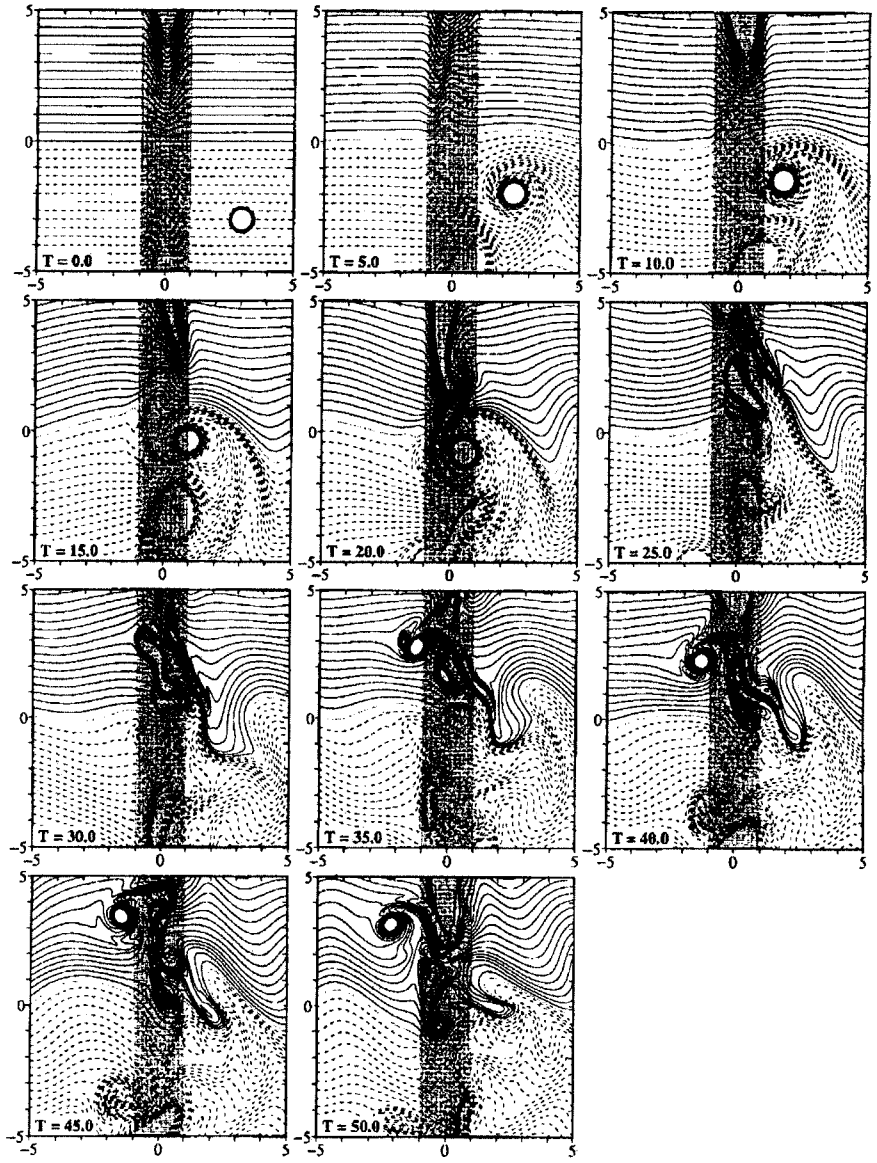

FIGURE 12 Contours of potential vorticity on the x, y-plane of a Bessel monopole that encounters a ridge like (20) with $A = 0.2$ and $w = 1.0$ along the y-axis (shaded region). Contour levels as in Figure 6.

Once the monopole has gathered enough positive potential vorticity around it, it can cross the top of the ridge, which it does at about $T = 25$. Due to a rather large shear on the monopole's north-east side, it is deformed strongly and splits into two parts between $T = 30$ and 35. The front part strengthens as it descends the ridge and manages to

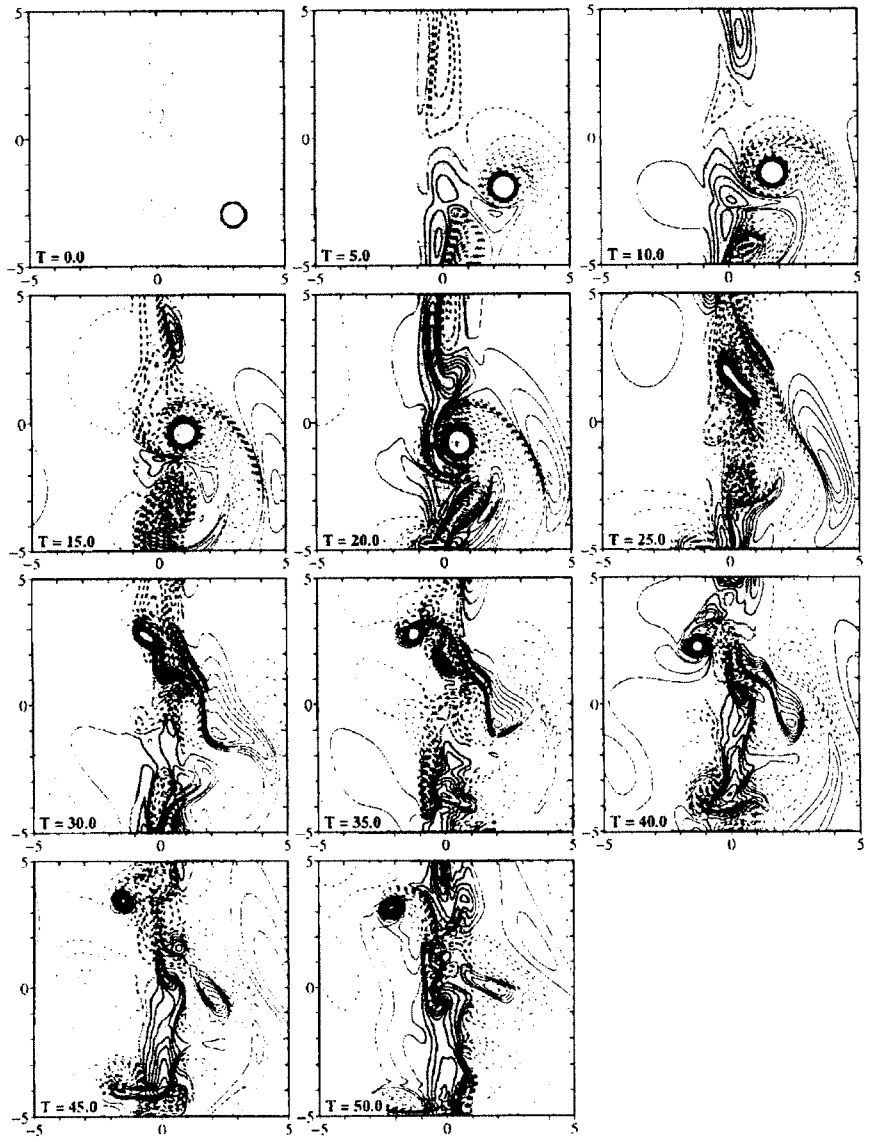

FIGURE 13 Contours of relative vorticity on the x, y-plane of the case shown in Figure 12. Contour levels as in Figure 6.

get clear from the ridge, followed by the usual north-west motion induced by the β-effect. The smaller trailing vortex visible at $T = 35$ seems somehow stuck on top of the ridge: it is too weak to descend the ridge permanently and it is torn apart by the strong shear in the "tail" of the leading vortex.

At $T = 20$, when the vortex is still on the east side of the ridge, the maximum of vorticity ω_{max} is clearly located at the centre of the monopole. As the vortex moves to the north, so does ω_{max}. At some point between $T = 25$ and 30, when the deformed vortex has partly crossed the top of the ridge, the location of ω_{max} is suddenly at the west side of the ridge, when that part of the vortex has become stronger than the trailing part. The trajectory of ω_{max}, plotted in Figure 14, therefore shows a "jump". The maximum of vorticity, given in Figure 15 as a function of time, reaches a minimum value at the moment of this jump. Due to the loss of a part of the vortex while crossing the ridge, the monopole is damaged and apparently this results in a lower ω_{max} than expected from viscous decay (Fig. 15). Yet, the position at $T = 50$ is not so very different from the ridge-less case.

7.2. Ridges of Different Widths

A north-south ridge clearly can have a significant effect on a monopole trying to cross it. In order to investigate the interaction more closely, consider first of all a change in the width of the ridge, with ω ranging from 0.25 to 2.0 in steps of 0.25 (the total width of the ridge

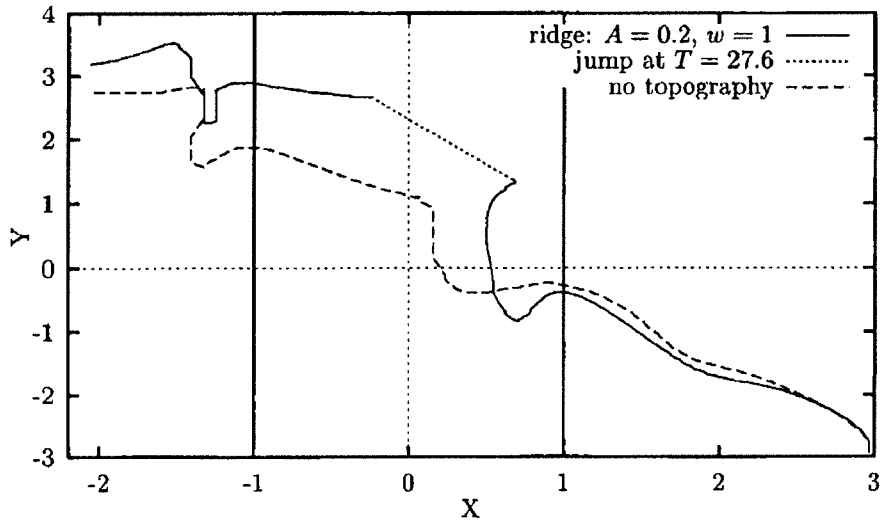

FIGURE 14 Trajectory of the maximum of vorticity of the Bessel monopole of Figure 12 (solid line) and its trajectory in the absence of the ridge (dashed line). The dotted line piece in the solid line indicates that the location of ω_{max} jumps from the right to the left side of the ridge at $T = 27.6$. The thick vertical lines mark the edges of the ridge.

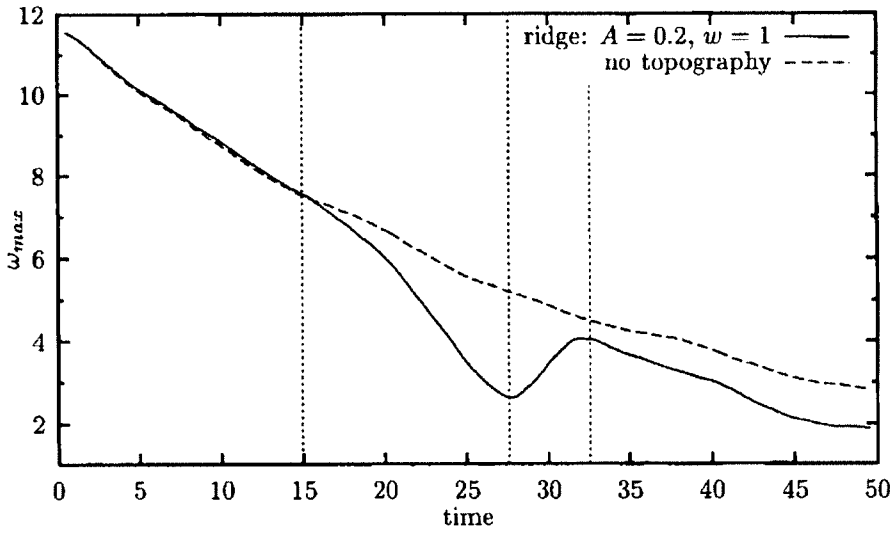

FIGURE 15 The maximum of vorticity as a function of time for the Bessel monopole whose trajectory is shown in Figure 14. Vertical lines represent the moments in time when the maximum of vorticity crosses the edges and the top of the ridge.

is $2w$; see Fig. 1) for $A = 0.2$. Figure 16 shows plots of the potential vorticity ω_p at $T = 30$ for all w-values and Figure 17 shows trajectories of the maximum of vorticity $\omega_{\max}$ for selected w-values.

For the case $w = 0.25$, the diameter of the monopole is twice the full width of the ridge. The ridge affects the monopole slightly (Fig. 16) but its trajectory (Fig. 17) is much like the ridge-less case except for an increase in the westward velocity of the monopole. As w increases to $w = 0.50$, the width of the ridge and the diameter of the monopole are almost the same (due to viscous effects the monopole has grown a little when it reaches the ridge) and, in this case, the monopole is clearly split into two portions (Fig. 16). The trajectory of $\omega_{\max}$ (Fig. 17) is quite different from the ridge-less case and as in Figure 14 for $w = 1.0$, it shows a jump. In fact, this case looks rather much like the $w = 1.0$ case of Figures 12–15. The trailing vortex visible in Figure 16 does not manage to cross the ridge before it is dissipated.

A ridge slightly wider than the monopole (see the case with $w = 0.75$ in Fig. 16) does deform the vortex but there is no splitting into two parts. The trajectory of $\omega_{\max}$ (not shown) is quite complicated, with an Ω-shaped turn at the west-edge of the ridge. At $T = 50$, however, the position is almost the same as for $\omega = 0.50$ and $\omega = 1.0$.

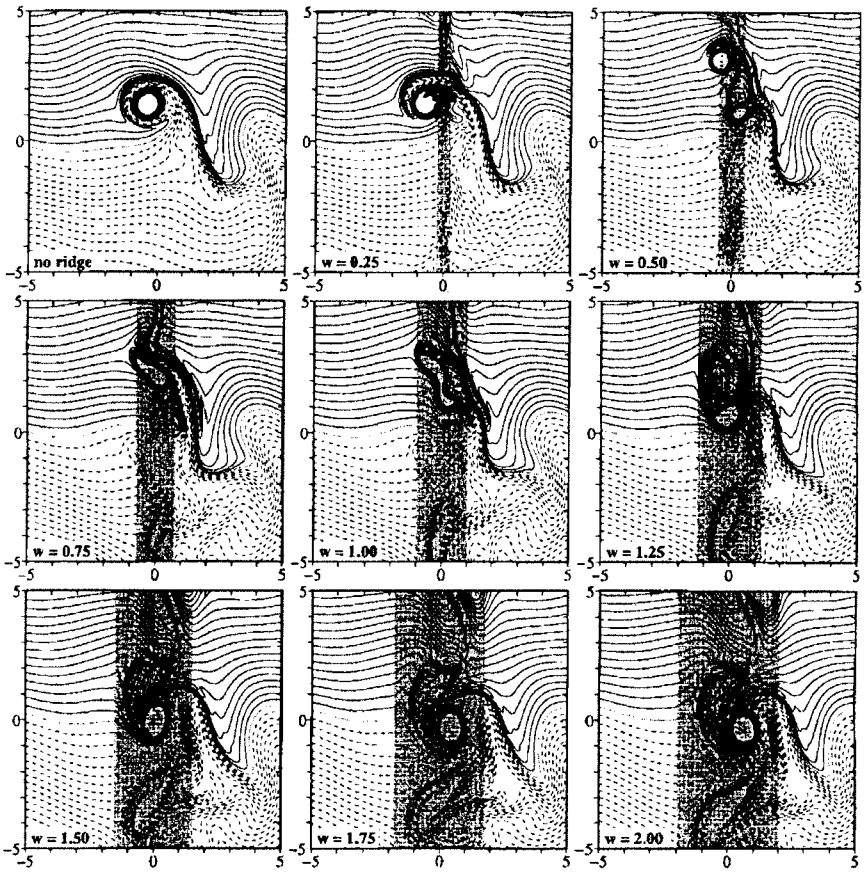

FIGURE 16 Contours of potential vorticity on the x, y-plane at $T = 30$ of a Bessel monopole that encounters a ridge like (20) along the y-axis with $A = 0.2$ for various widths of the ridge (shaded region) and for the ridge-less case (top-left). Contour levels as in Figure 6.

The case of $w = 1.00$, discussed in more detail above, leads to a splitting of the vortex as for $w = 0.50$, but unlike the $w = 0.75$ and $w = 1.25$ cases. For the latter case, where the ridge is about twice as wide as the monopole, the vortex is deformed considerably (Fig. 16), leaving behind a trail of vorticity, but without a secondary vortex being formed. The trajectory of $\omega_{\max}$ (not shown) lies between the trajectories for $w = 0.25$ and $w = 1.50$ (Fig. 17) and at the west-edge of the ridge it shows a loop that is larger than for $w = 1.50$. The position at $T = 50$ lies near the penultimate bend in the $w = 0.25$-trajectory.

For $w = 1.50$, the deformation of the monopole due to the ridge is less than the deformation for smaller w-values. At $T = 30$ (Fig. 16), the

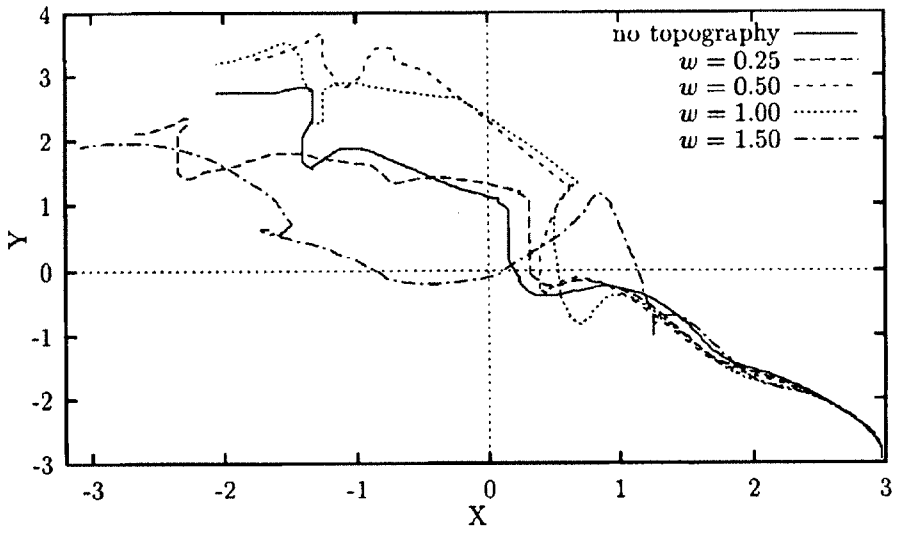

FIGURE 17 Trajectories of the maximum of vorticity of a Bessel monopole that encounters a ridge like (20) along the y-axis with $A = 0.2$ and selected values for w, as well as its trajectory in the absence of the ridge.

vortex is on the top of the ridge, with a trail of vorticity behind it (which does not lead to a secondary vortex). After $T = 30$, the vortex descends the ridge at the west, performs a small loop near the edge and then goes westward (Fig. 17).

Figure 16 shows that for a wide ridge, such as $w = 1.75$ and $w = 2.00$, the deformation of the monopole is less than for smaller ridges, a feature that is true for $T < 30$ also. But the centre of the monopole is still at the east side of the ridge. Subsequently – see Figure 18 – the vortex undergoes another deformation, and then restores itself (at $T = 40$), but it still has not passed the top of the ridge completely. Another deformation follows and, by then, the vortex is so weak that it does not survive: it is destroyed by the vorticity induced by the ridge.

In all these cases the initial position of the monopole is the same: (3,−3). This means that when the vortex reaches the edge of the ridge it is not in all cases of the same size and strength because of viscous effects. Consider instead initial positions such that the centre of the monopole is always 2 length units from the edge of the ridge (no graphs of these simulations are shown). For the narrower ridges, $w \leq 1$, the difference in evolution is not significant, though the forms of the deformations are slightly different. For wider ridges, $w > 1$, there is

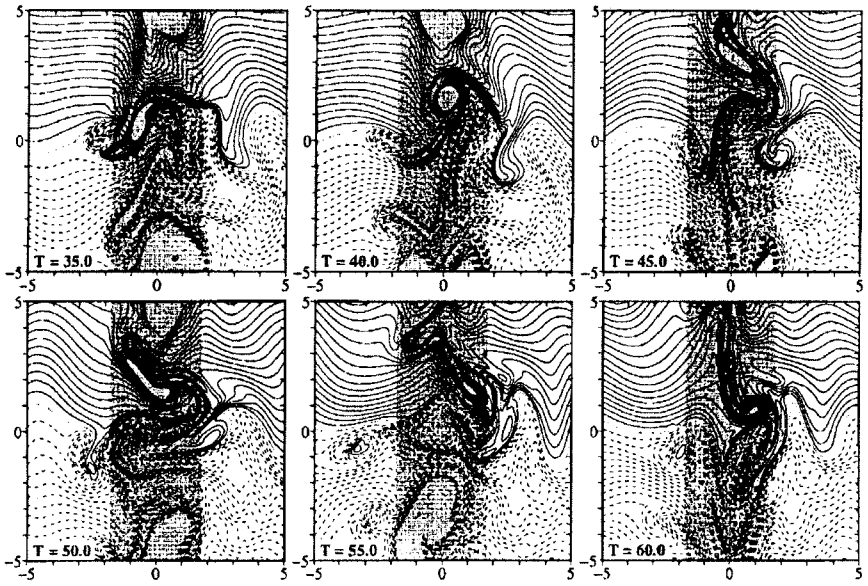

FIGURE 18 Contours of potential vorticity on the x, y-plane of a Bessel monopole that encounters a ridge like (20) with $A = 0.2$ and $w = 1.75$ along the y-axis (shaded region). Contour levels as in Figure 6.

a bigger difference. Ridges with $w = 1.25$ and $w = 1.50$, for instance, are too wide for the monopole to cross before it decays due to viscosity. And for larger w-values the vortex is dissipated at earlier times. This indicates that viscosity plays an important role in the evolution of the vortex–topography interaction.

7.3. Effect of a Lower Viscosity

Reducing the viscosity has two notable effects: the strength of the monopole reduces less fast and the low-level vorticity induced by the ridge, the Rossby-waves and the motion of the vortex across the grid decays slower. To see the effect of this on the monopole's evolution, the same simulations as above are made at Re = 10,000 [with the monopole always starting from (3, −3) again]. Using a 256×256 grid for these simulations is not enough since a 512×512 gives significantly different results when there is a ridge in the domain, so the latter grid is used (with time step $\Delta_t = 0.025$). Perhaps an even denser grid is desirable, but for computational reasons this option is not feasible.

(Using a 512 × 512 grid for the Re = 1000 simulations proved to make little difference).

Figure 19 shows contours of potential vorticity at $T = 30$ for all the ω-values and Figure 20 shows the trajectory of the maximum of vorticity for some ω-values. These graphs can be compared directly with Figures 16 and 17 for Re = 1000, respectively. The vortex survives crossing the ridge in all cases, with the formation of a secondary vortex for $w = 0.50$, 0.75 and 1.0. The trajectories are more complicated, as can be seen from Figure 20. At $T = 50$, the vortices are located south-west of the vortex in the ridge-less case, except for $w = 0.75$ (not shown): then the vortex is just north of the ridge-less case. For ridges with $w > 1$ the positions at $T = 50$ are quite close

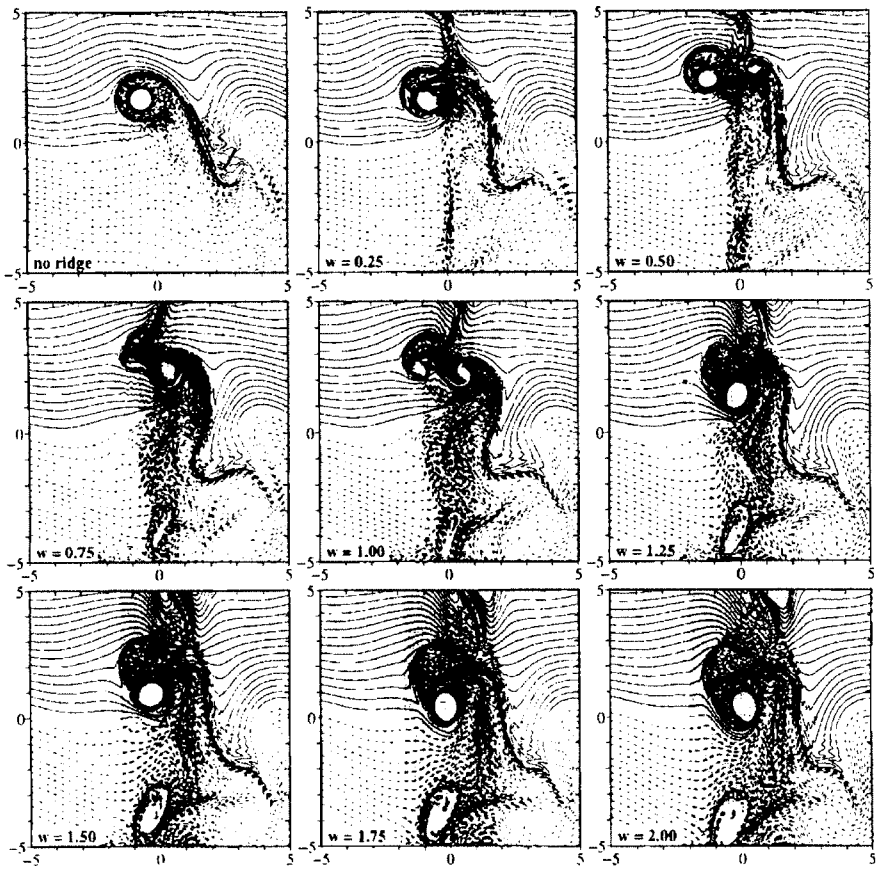

FIGURE 19 Contours of potential vorticity on the x, y-plane at $T = 30$ of a Bessel monopole that encounters a ridge like (20) along the y-axis with $A = 0.2$ for various widths of the ridge (shaded region) and for the ridge-less case (top-left), for Re = 10,000. Contour levels as in Figure 6.

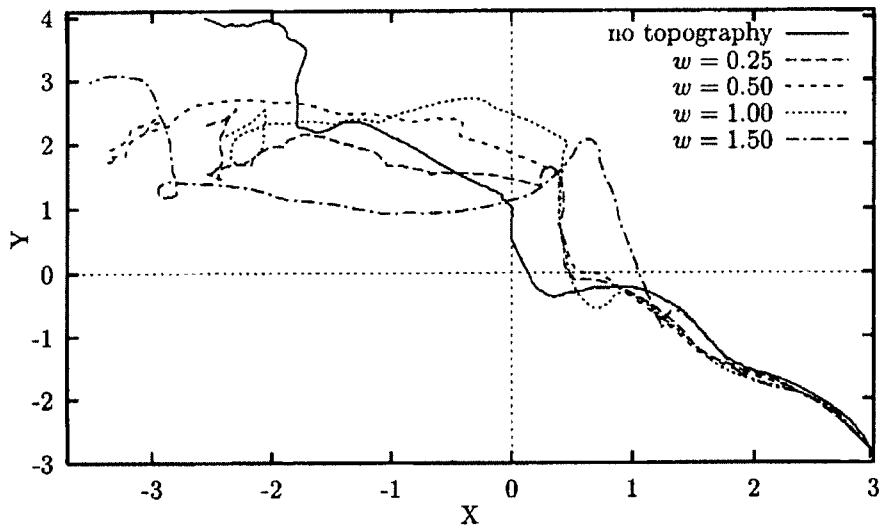

FIGURE 20 Trajectories of the maximum of vorticity of a Bessel monopole that encounters a ridge like (20) along the y-axis with $A = 0.2$ and selected values for w, as well as its trajectory in the absence of the ridge, for Re = 10,000.

together (see $w = 1.50$ in Fig. 20). There are more bends and loops in the trajectories than in Figure 16 due to the presence of the vorticity induced by the ridge and Rossby-waves. A brief summary of the case study results is as follows.

$w = 0.25$ There is, as with the Re = 1000 case, little deformation when the vortex crosses the ridge. The vorticity shed by the monopole, visible in Figure 19, does not lead to a secondary vortex and the monopole crosses the ridge without much damage. The maximum of vorticity ω_{max}, however, is after it crossed the ridge (around $T = 30$) higher than expected from viscous decay without a ridge, as can be seen in Figure 21 (for Re = 1000 this is not the case). The reason for this increase in ω_{max} is unclear, but it is evidently associated with the reduction in size of the monopole. This excess in ω_{max} decays relatively fast and at $T = 50$ it is only a little higher than expected.

$w = 0.50$ At $T = 30$ (Fig. 19), a secondary vortex is formed at the east side of the ridge, originating from a splitting of the initial vortex as it crosses the top (shortly after $T = 25$). The

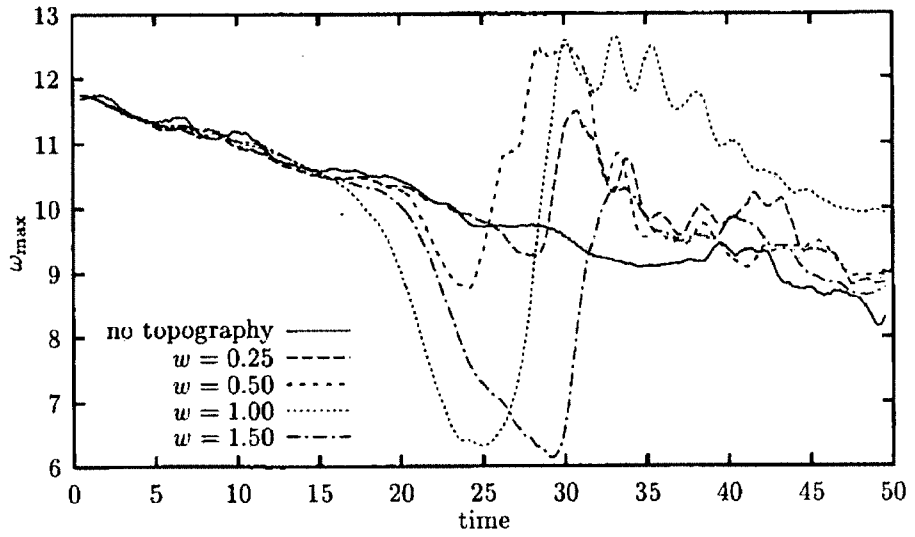

FIGURE 21 The maximum of vorticity as a function of time of the Bessel monopoles whose trajectories are shown in Figure 20.

leading vortex (where ω_{max} within the domain is located) moves away from the ridge after $T = 30$ along a complex curved path. The secondary vortex manages to cross the top of the ridge as well, but it is not yet free from the ridge at $T = 50$.

$w = 0.75$ The monopole is slightly smaller than the ridge when it crosses the top (at about $T = 25$) and there is a deformation similar to the case with Re = 1000, but now a secondary vortex is formed in the wake of the main vortex on the west side of the ridge. This secondary vortex follows the leading one on its north-west path.

$w = 1.00$ This case again looks more like $w = 0.50$ than like $w = 0.75$ and a clear secondary vortex is formed on the east side of the ridge. This secondary vortex, which seems to be of the same size as the leading vortex, also crosses the top of the ridge, but is not free from the ridge at $T = 50$. The value of ω_{max} (Fig. 21) shows an oscillatory behaviour after it has reached a peak value when located at the edge of the ridge (just before $T = 40$).

$w = 1.25$ This ridge deforms the monople somewhat as it crosses the top, but there is no sign of a secondary vortex being formed. At $T = 30$ (Fig. 19), the monopole is at the top of the ridge.

From there, it moves westward away from the ridge before going somewhat more to the north-west after $T = 40$.

$w = 1.50$ This case looks similar to $w = 1.25$, except that the trajectory of ω_{max} (Fig. 20) lies after it has crossed the ridge first more to the south and then to the west of the $w = 1.25$-trajectory, though the positions at $T = 50$ are not far apart. Again, the value of ω_{max} west of the ridge is higher than expected from viscous decay (Fig. 21), but not as high as for lower w-values.

$w = 1.75$ and $w = 2.00$ These two cases are rather alike, leaving the ridge slightly more to the south than $w = 1.50$, but meeting near the same point at $T = 50$.

7.4. Ridges with Different Heights

The ridges along the y-axis discussed above all have $A = 0.2$ in (20), which means that the maximum height of the ridge is $2A = 0.4$. Compared with the default fluid depth $H = 1$ this is probably about the maximum value of A allowed for the assumption of 2D motions to remain valid. Therefore, only smaller A-values ($A = 0.15$, 0.1 and 0.05) are investigated. For all these cases, at every w-value used above, the monopole appears to be able to cross the ridge. For $A = 0.15$, deformations in the shape of the vortex are visible at $T = 25-30$, but the monopole recovers from this, without an indication of splitting into two parts. For lower values of A deformations are hardly visible. Hence, a ridge with $A = 0.2$ is much more disturbing for the monopole than lower ridges.

Figure 22 presents, as an example, the trajectories of the maximum of vorticity ω_{max} for $w = 1.0$ (with Re = 1000 again). For low ridges, these trajectories do not differ significantly from each other. For $A = 0.15$, ω_{max} performs a loop just before crossing the top of the ridge, in contrast to the cases for lower values of A, where there is no such loop near the top, but there is a rather sharp turn to the west. Near the western edge of the ridge there is a loop in the trajectory for all three cases. For $A = 0.2$ the trajectory is quite different from the other cases and it shows no loop, only a kind of Ω-turn west of the ridge (see also Fig. 13). Even a very low ridge (see for example $A = 0.05$)

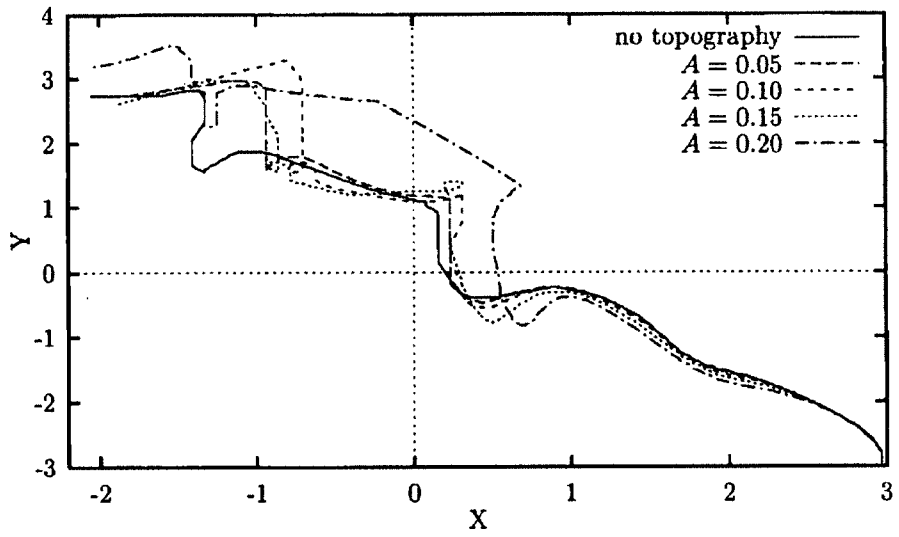

FIGURE 22 Trajectories of the maximum of vorticity of a Bessel monopole that encounters a ridge like (20) along the y-axis with $w = 1.0$ and several values for A, as well as its trajectory in the absence of the ridge.

clearly affects the trajectory of the monopole, especially near the western edge of the ridge.

As for the value of ω_{max} for these cases: there is a small decrease for $A = 0.05$ and 0.1 when the monopole crosses the ridge, as expected, and ω_{max} recovers to the value expected from viscous decay quite well. For $A = 0.15$, the decrease in ω_{max} is bigger and shows a bump (like in Fig. 8) when the monopole performs the loop near the top of the ridge. When the monopole has left the ridge, ω_{max} is larger than expected from viscous decay: crossing the ridge has strengthened the vortex, (ω_{max} for $A = 0.2$ is shown in Fig. 14).

8. CONCLUDING REMARKS

The interaction of a monopolar vortex with a topographic ridge has been investigated with a two-dimensional numerical method. In the model, the (cyclonic) monopole, which is of Bessel type, moves through the domain to the north-west due to the so-called β-effect, i.e. the latitudinal variation of the Coriolis force: $f = \beta y$, with y the local north coordinate. As the monopole moves it leaves behind vorticity in the form of Rossby-waves and the monopole interacts with these

waves. Because of this interaction the monopole's trajectory is not a simple straight line to the north-west (see Fig. 5).

In the course of its motion through the domain, the monopole encounters a topographic ridge with a cosine shape (Fig. 1), oriented in different ways and with the possibility of having different heights and widths. From the results presented in this paper it is clear that the width and height of the ridge are important for what happens to a vortex that encounters the ridge. Even more important, however, is the orientation of the ridge, i.e. the degree to which the topography deforms the contours of potential vorticity from the β-effect, which lie equidistant from each other and parallel to the x-axis. The nature of the interactions occuring as the controlling parameters are varried is extremely complex, requiring a parametric case study approach to understand the associated dynamics.

A ridge along the x-axis causes only a minimal deformation of these contours and hence only a small disturbance in the trajectory of the monopole that encounters the ridge. It seems that the vortex can only cross the top of the ridge once it has positive potential vorticity sufficiently close to its (north)west side, and the vortex achieves this by moving westward along the ascending side of the ridge (Fig. 10). If the ridge is along the line $y = x$ the contours from the β-effect are deformed more and the monopole's trajectory differs more from the ridge-less case than for a ridge along the x-axis. In both cases, however, the vortex manages to cross the top of the ridge after gathering sufficient positive potential vorticity, even for very high and wide ridges ("very high" of course within the assumption of two-dimensional motions in the model).

A north-south oriented ridge causes considerable deformation of the contours from the β-effect: the local north coordinate induced by the ridge is directed uphill, i.e. perpendicular to the north coordinate of the β-effect. Because of this, such a ridge can have a more significant effect on the fate of the vortex, depending on the width and height, than the earlier ridges. There does not seem to be a simple criterion to distinguish different regimes of the monopole's evolution, but a few remarks can be made. For low ridges, the disturbance is minimal and for these low ridges the width is not of influence on the survival of the vortex; different widths lead, however, to slightly different trajectories after the monopole has crossed the ridge. Somewhat higher ridges

cause more disturbances in the monopole's trajectory and deform its shape more, but the vortex can cross the ridge.

For a very high ridge, with a height of 0.4 times the fluid depth away from the ridge, the results can be summarised as follows. A very narrow ridge (smaller that the size of the monopole) seems to have little effect on the monopole itself, though its trajectory is shifted somewhat. Wider ridges can deform the vortex so much that it splits into two parts when it crosses the top of the ridge (where the secondary vortex may or may not also cross the ridge). And for even wider ridges, 3 to 4 times the size of the monopole, the deformation can lead to the destruction of the monopole if the monopole is not strong enough (anymore). The latter condition also depends on the strength of the viscous effects.

Higher ridges no doubt lead to more deformations and the possible destruction of the monopole even for narrow ridges. In principle it is even possible that the relative vorticity changes sign when the monopole climbs the ridge. Let ω_0 and ω_h be the relative vorticity of the monopole away from the ridge and at height $h = 1 - H$, respectively. Conservation of potential vorticity (neglecting viscous effects for a moment) then implies that $\omega_h = \omega_0(1-h) - hf$. For a positive monopole a change of sign thus takes place if $h > \omega_0/(\omega + f)$. For a ridge with $f = 1/3$ this occurs if $\omega_0 < f/2 = \beta y/2$. This means either a very weak monopole, or a strong β-effect or a very large y-value – all of which seems not realistic within the model. The higher the ridge, the more plausible such a change of sign. But since a height of 0.4 seems to be about the maximum allowed height within the assumption of two-dimensional motions, this cannot be investigated with the model.

The computations described in this paper are performed with a monopole of radius 0.5 in a 20×20 domain. If a larger domain is used, two effects influence the evolution of the monopole. A detailed study of this point falls outside the scope of the present paper, but a few remarks are in order. As noted in Section 4.1, the trajectory of the monopole will show a difference in the number and location of the bends caused by the interaction with the Rossby-waves. Without any topography, this has no significant effect on the average motion of the monopole. If the monopole encounters a ridge, however, there will be a difference in the evolution since the monopole will reach the ridge at

a slightly different location under a somewhat different angle because of the bends in its trajectory. Hence, the interaction of the monopole with the ridge-induced relative vorticity – clearly visible north and south of the monopole in, for example, Figure 13 – will be a little different. A larger domain also means that for a north-south ridge the generation of relative vorticity at the ridge near the boundaries will be stronger, since this depends on the north-south coordinate y, that is on the degree in which the ridge deforms the contours of potential vorticity of the β-effect, which is more for larger $|y|$. Since this stronger ridge-induced relative vorticity is at the same time further away from the centre of the domain (where the monopole's evolution takes place), the effect on the monopole's evolution is less than the effect of the vorticity induced by the ridge near the monopole. The combined effect of a slightly different approach of the north-south ridge by the monopole and the stronger ridge-induced vorticity further away (for larger $|y|$) is that there will be a small difference in the monopole's evolution if a larger domain is used. But there is no indication that a larger domain means better or more accurate results, since the relative vorticity at the ridge is generated by the ridge, not by the boundaries of the domain. A 20×20 domain is thus sufficiently large and the results should be considered with respect to this domain.

In all cases when the monopole actually crosses the top of the ridge, it can only do so after it has gathered sufficient positive potential vorticity on its (north)west side. For a north-south ridge, the vortex achieves this by going north along the ascending (east) side of the ridge (Fig. 12). The computations discussed in this paper are made on a pure β-plane, with $f = f_0 + \beta y = \beta y$, which means that the domain has a part with negative ($y < 0$) and a part with positive ($y > 0$) potential vorticity when the monopole approaches the ridge (see for instance the top-left panel of Fig. 12). In other words, the ridge is centred on the equator ($y = 0$), where f changes sign. It therefore seems likely that the fate of the monopole also depends on the initial y-position of the vortex. This point is currently under study and results will be presented elsewhere.

Another point that will be addressed is the effect of a non-zero f_0 in the Coriolis parameter $f = f_0 + \beta y$. For motions in the absence of topography the value of f_0 does not matter since it is a constant that drops out of the equations: it only appears in derivatives. If the fluid

depth H does depend on position, however, this is no longer the case since the potential vorticity $\omega_p = (\omega + f)/H$ appears in the derivatives. The value of f_0 will therefore matter for the evolution of the monopole when it is on the ridge and hence f_0 may determine the actual fate of the vortex.

Acknowledgements

The authors would like to thank G. J. F. van Heijst for many useful discussions and suggestions. The research described in this paper is financed by the TMR-MAST programme of the European Union (MAS3-CT96-5012, DG12-ASAL); the authors gratefully acknowledge this support.

References

Arakawa, A., "Computational design for long-term numerical integration of the equations of fluid motion: two-dimensional incompressible flow. Part I," *J. Comp. Phys.* **1**, 119–143 (1966).

Bograd, S. J., Rabinovich, A. B., LeBlond, P. H. and Shore, J. A., "Observations of seamount-attached eddies in the North Pacific," *J. Geophys. Res.* **102**(C6), 12,441–12, 456 (1997).

Bower, A. S., Armi, L. and Ambar, I., "Direct evidence of meddy formation off the southwestern coast of Portugal," *Deep-Sea Res.* **42**, 1621–1630 (1995).

Carnevale, G. F., Kloosterziel, R. C. and Van Heijst, G. J. F., "Propagation of barotropic vortices over topography in a rotating fluid," *J. Fluid Mech.* **233**, 119–139 (1991).

Carnevale, G. F., Vallis, G. K., Purini, R. and Briscolini, M., "Propagation of barotropic modons over topography," *Geophys. Astrophys. Fluid Dynam.* **41**, 45–101 (1988).

Chaplygin, S. A., "One case of vortex motion in fluid," *Trans. Phys. Sect. Imperial Moscow Soc. Friends of Natural Sciences* **11**(N 2), 11–14. Also in *Collected Works*, 1948, vol. 2, pp. 155–165 (1903) (in Russian).

Ezer, T., "On the interaction between the Gulf Stream and the New England seamount chain," *J. Phys. Ocean.* **24**, 191–204 (1994).

Grimshaw, R., Broutman, D., He, X. and Sun, P., "Analytical and numerical study of a barotropic eddy on a topographic slope," *J. Phys. Ocean.* **24**, 1587–1607 (1994).

Hockney, R. W., "A fast direct solution of Poisson's equation using Fourier analysis," *Journal of the Association for Computing Machinery* **12**, 95–113 (1965).

Kamenkovich, V. M., Leonov, Y. P., Nechaev, D. A., Byrne, D. A. and Gordon, A. L., "On the influence of bottom topography on the Agulhas eddy," *J. Phys. Ocean.* **26**, 892–912 (1996).

Korotaev, G. K. and Fedotov, A. B., "Dynamics of an isolated barotropic eddy on a beta-plane," *J. Fluid Mech.* **264**, 277–301 (1994).

Lamb, H., *Hydrodynamics*, 6th edition, Cambridge University Press, Cambridge (1932).

Mc Williams, J. C., Gent, P. R. and Norton, N. J., "The evolution of balanced, low-mode vortices on the β-plane," *J. Phys. Ocean.* **16**, 838–855 (1986).

Meleshko, V. V. and Van Heijst, G. J. F., "On Chaplygin's investigations of two-dimensional vortex structures in an inviscid fluid," *J. Fluid Mech.* **272**, 157–182 (1994).

NAG manual, Chapter D03: Partial Differential Equations.

Orlandi, P., "Vortex dipole rebound from a wall," *Phys. Fluids A* **2**, 1429–1436 (1990).

Richardson, P. L., "Tracking ocean eddies," *American Scientist* **81**, 261–271 (1993a).

Richardson, P. L., "A census of eddies observed in North Atlantic SOFAR float data," *Prog. Oceanog.* **31**, 1–50 (1993b).

Shapiro, G. I., Meschanov, S. L. and Emelianov, M. V., "Mediterranean lens 'Irving' after its collison with seamounts," *Oceanologica Acta* **18**(3), 309–318 (1995).

Smith IV, D. C. and O'Brien, J. J., "The interaction of a two-layer isolated mesoscale eddy with bottom topography," *J. Phys. Ocean.* **13**, 1681–1697 (1983).

Sutyrin, G. G., Hesthaven, J. S., Lynov, J. P. and Juul Rasmussen, J., "Dynamical properties of vortical structures on the beta-plane," *J. Fluid Mech.* **268**, 103–131 (1994).

Van Geffen, J. H. G. M., *Documentation of the software package NSEVOL*, Report R-1466-D, Eindhoven University of Technology (1998).

Van Geffen, J. H. G. M. and Van Heijst, G. J. F., "Viscous evolution of 2D dipolar vortices," *Fluid Dynam. Res.* **22**, 191–213 (1998).

Van Geffen, J. H. G. M., Meleshko, V. V. and Van Heijst, G. J. F., "Motion of a two-dimensional monopolar vortex in a bounded rectangular domain," *Phys. Fluids* **8**, 2393–2399 (1996).

Van Heijst, G. J. F., "Topography effects on vortices in a rotating fluid," *Meccanica* **29**, 431–451 (1994).

Velasco Fuentes, O. U. and Van Heijst, G. J. F., "Experimental study of dipolar vortices on a topographic β-plane," *J. Fluid Mech.* **259**, 79–106 (1994).

Verron, J. and Le Provost, C., "A numerical study of quasi-geostrophic flow over isolated topography," *J. Fluid Mech.* **154**, 231–252 (1985).

Verzicco, R., Flór, J.-B., Van Heijst, G. J. F. and Orlandi, P., "Numerical and experimental study of the interaction between a vortex dipole and a circular cylinder," *Exp. Fluids* **18**, 153–163 (1995).